Die-Level Glass Frit Vacuum Packaging for a Micro-Fuel Processor System

by

Kerry Cheung

B.S., Applied and Engineering Physics
Cornell University, 2003

Submitted to the Department of Electrical Engineering and Computer Science
in Partial Fulfillment of the Requirements for the Degree of

Master of Science in Electrical Engineering and Computer Science

at the

MASSACHUSETTS INSTITUTE OF TECHNOLOGY
June 2005

© 2005 Massachusetts Institute of Technology
All rights reserved

Signature of Author: ______________________________
Department of Electrical Engineering and Computer Science
May 20, 2005

Certified by: ______________________________
Martin A. Schmidt
Professor of Electrical Engineering and Computer Science
Thesis Supervisor

Accepted by: ______________________________
Arthur C. Smith
Chairman, Committee on Graduate Students

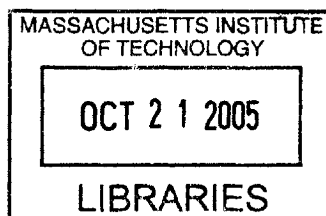
MASSACHUSETTS INSTITUTE OF TECHNOLOGY
OCT 2 1 2005
LIBRARIES

BARKER

Die-Level Glass Frit Vacuum Packaging for a Micro-Fuel Processor System

by

Kerry Cheung

Submitted to the Department of Electrical Engineering and Computer Science
on May 20, 2005 in Partial Fulfillment of the Requirements for the Degree of
Master of Science in Electrical Engineering and Computer Science

Abstract

Vacuum packaging utilizing glass frit is investigated for the use with a micro-fuel processor. Enhanced device performance through proper thermal management motivates the need for a vacuum package on the micro scale. Constraints imposed by the design and fabrication of the micro-fuel processor deem glass frit bonding as the optimal method for packaging.

The quality of the glass seal is dependent on the pre-sintering process as well as bonding parameters. Ideal pre-sintering of a lead-zinc-borosilicate glass tape, GPR-10 from Vitta Corp., has been achieved, and a vacuum bonding technique was optimized. The seal quality is determined visually with microscopy by comparing the size and quantity of voids present in the frit layer post-bonding. A package with a vacuum of <150mTorr was obtained but the seal quickly degraded.

A new packaging scheme utilizing a two-step bond process is developed and evaluated. Bond optimization is applied to this process resulting in a hermetically sealed package. Hermeticity was not lost after heating the package at 450°C for 30+ hours. Final seal-off in a vacuum chamber was attempted with glass powders, glass preforms, and solders to no avail but preliminary results with solder appears promising.

Despite unsuccessfully producing a vacuum package, the methodology for optimizing bonding parameters can be utilized for glass frits that possess different physical properties from GPR-10. The two step process developed is quite versatile and permits the use of bonding technologies that was considered incompatible previously. There is confidence that a vacuum package can be achieved if the additional work described is conducted.

Thesis Supervisor: Martin A. Schmidt
Title: Professor of Electrical Engineering and Computer Science

Acknowledgements

First, I would like to express my gratitude to Professor Martin A. Schmidt and Professor Klavs F. Jensen for providing me with the opportunity to conduct research under their supervision. Their continual guidance through suggestions, advice, and feedback made this experience extremely educational.

Deep appreciation goes to all the members of the Schmidt group for their help, support, and friendship, especially Ole Nielson and Antimony Gerhardt. I would also like to thank Ben Wilhite, Steve Weiss, and Smitha Matthews for their assistance, other members of the MURI project who provided input, and the staff of MTL who trained and assisted me with fabrication.

Last but not least, I am eternally grateful to my family for always believing in me and providing ceaseless encouragement, and to the friends I have made at MIT who made my time here quite enjoyable. This thesis is dedicated to you all.

Table of Contents

List of Figures 9
List of Tables 9
1 – Introduction 11
2 – Background 13
2.1 – Packaging and Evaluation 13
2.2 – Bonding Techniques 13
2.3 – Vacuum Sensing 15
3 – Bond Optimization 17
3.1 – Motivation and Approach 17
3.2 – Pre-sintering Parameters 18
3.3 – Bonding Parameters 21
3.4 – Results 23
4 – Two-Step Bond Approach 25
4.1 – Motivation 25
4.2 – Packaging Concept 25
4.3 – Cap Design 26
4.4 – Final Seal-off 28
5 – Device and Fabrication 31
5.1 – Device Overview 31
5.2 – Capping Dies 31
5.3 – Device Layer 32
5.4 – Two-Step Bond Cap 33
6 – Experimentation 35
6.1 – Calibration 35
6.2 – Frit Transfer 38
6.3 – Vacuum Bonding 39
6.3.1 – Setup 39
6.3.2 – Results 41
6.4 – Two-Step Bonding 44
6.4.1 – Setup 44
6.4.2 – Results 46
7 – Future Work 49
8 – Conclusions 51
Appendix A – Modeling of Sensor 53
Appendix B – Non-Evaporable Getters (St122) 58
Appendix C – Process Flows 60
Appendix D – Mask Layouts 63
Appendix E – Technical Drawings 67
Appendix F – Optimization Images 70
References 89

List of Figures

Figure 1-1. Suspend Tube Microreactor 11
Figure 1-2. Experimental Heat Loss of Tube Microreactor 12
Figure 3-1. Rough Glazed Surface with Cracks 19
Figure 3-2. Comparison of Initial Pre-sinter and Optimized Pre-sinter 20
Figure 3-3. Visualization of a Good Bond 22
Figure 3-4. Results of Bond Optimization 23
Figure 4-1. Schematic Diagram and Picture of a Packaged FED Panel 25
Figure 4-2. Schematic for Two-Step Process 26
Figure 4-3. Design of Bottom Cap 27
Figure 4-4. Three Different Cap Designs 28
Figure 5-1. Overall Packaged Device Schematic 31
Figure 5-2. Fabrication Steps for the Top and Bottom Caps 32
Figure 5-3. Fabrication Steps for the Device Layer 33
Figure 5-4. Fabrication Steps for Two-Step Bond Cap 33
Figure 6-1. Four-point Probe Chuck 35
Figure 6-2. Reliability Test of Glass Frit Bonds 36
Figure 6-3. Reliability Test of Sensor After E-beam 37
Figure 6-4. Frit Transfer Methodology 39
Figure 6-5. Vacuum Bond Setup 40
Figure 6-6. New Chuck and Cartridge Heaters 41
Figure 6-7. Misleading Glass Frit Bond 42
Figure 6-8. Experimental Result Showing Leaky Vacuum Package 43
Figure 6-9. SEM of Optimized Bond 43
Figure 6-10. Machined Bonding Chuck and Shadow Mask 44
Figure 6-11. Modified Heating Cycle 45
Figure 6-12. Box Furnace Bond Setup 45
Figure 6-13. Final Seal-Off Setup 45
Figure 6-14. Final Seal-Off with Low Melting Glass 46
Figure 6-15. Final Seal with Solder 47
Figure 6-16. Gold-Tin Seal-Off with Extended Outgassing 48
Figure 7-1. Potential Seal-Off Scheme 49
Figure 7-2. Glass Tube Brazing 50

List of Tables

Table 3-1. Physical Properties of GPR-10 17
Table 3-2. Presintering Trials 18
Table 3-3. Bonding Parameter Sets 21
Table 4-1. Physical Properties of Seal-Off Materials 29

Chapter 1
Introduction

The demand for portable power has grown substantially in our technologically advanced society. From consumer electronics to military weaponry, high density compact power has become a necessity. Current portable power sources are dominated by lithium-ion batteries but this technology may soon fall short of the need for larger and larger power densities. An attractive solution is to take advantage of the linearly scalable functional densities associated with MEMS devices.

Fuel cells, turbines, thermoelectrics, and thermophotovoltaics are several power generation schemes that are currently being implemented with microfabrication techniques. In our group, micro-fuel processor systems under development are focused around fuel cells and thermophotovoltaics. At the core of these systems is a suspended tube microreactor that has a basic schematic shown in Figure 1-1. The tube reactor is designed for the thermal decomposition, or cracking, of methanol or ammonia into hydrogen that is then fed into a fuel cell for power generation. Additionally, this reactor can be used to combust chemical fuels to produce heat and radiation for conversion into electricity through the utilization of photocells.

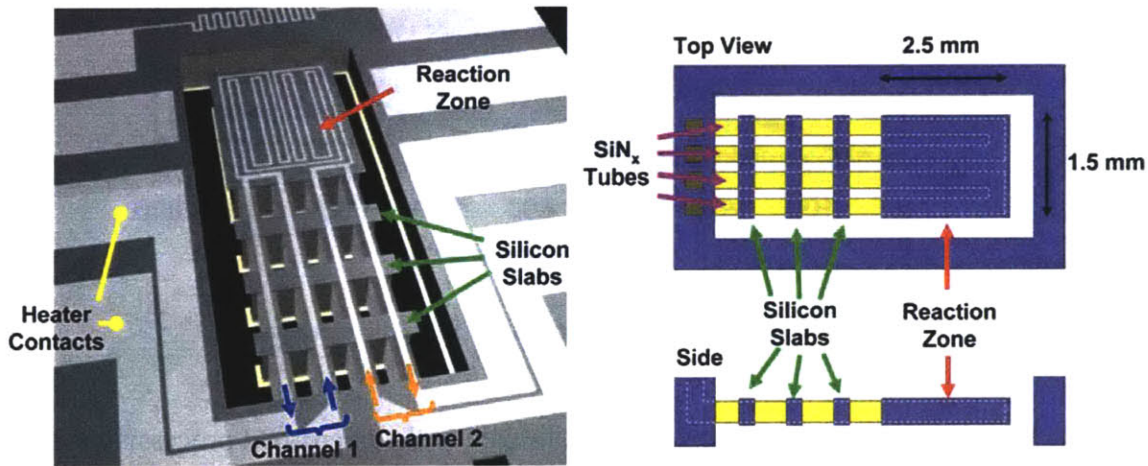

Figure 1-1. Suspend Tube Microreactor [1]

Thermal management is a key factor that greatly affects the efficiency of these fuel processing systems. Excessive heat loss in the microreactor will decrease the temperature of the reaction zone, resulting in an inefficient cracking reaction or reduced emission of radiation in combustion mode. Another issue for a thermophotovoltaic configuration is the degradation of photocell performance with increasing temperatures. Clever design and intelligent material choices can be utilized to minimize the solid heat conduction away from the reaction zone but a significant amount of heat will still be lost by conduction through air.

Figure 1-2 shows experimental data for the steady state heat loss versus operating temperature of a suspended tube reactor functioning in air and in a vacuum environment. Individual components of the heat loss such as air conduction and convection, radiation, and solid conduction are identified and plotted as well. From the graph, we see that air conduction and convection accounts for approximately 60% of the total heat loss of the device at the desired operation temperature of 800°C. A straight forward solution to this problem is to eliminate the heat loss pathways associated with air by utilizing a vacuum package.

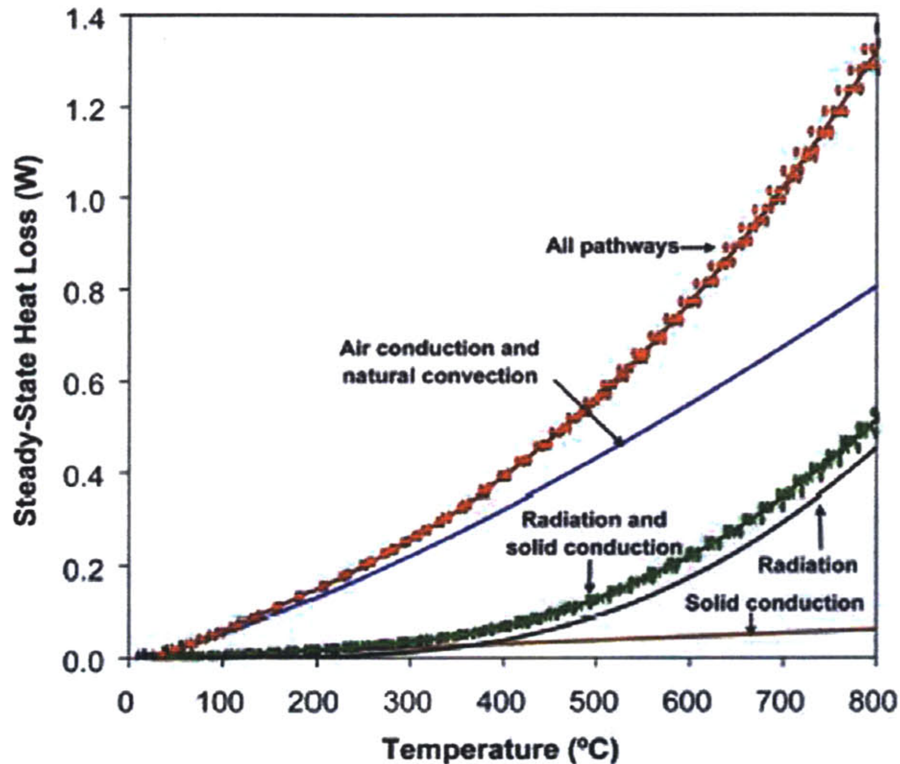

Figure 1-2. Experimental Heat Loss of Tube Microreactor [1]

Vacuum packaging technology is not limited to the micro-fuel processing systems currently researched in our group. Once a viable packaging scheme is developed for our microreactor, it can be applied to accelerometers, display panels, and other devices where a vacuum environment is crucial for ideal performance. Furthermore, this packaging technology can be applied to devices that require hermetic seals such as digital mirror displays or differential pressure sensors.

Chapter 2
Background

2.1 – Packaging and Evaluation

Several methods of vacuum packaging have been frequently used in industry and research. Silicon fusion bonding, anodic bonding, and intermediate material bonding using glass frit, solder, or gold, have been reported as promising methods for packaging applications [2-6]. Despite all these options, the current design for the microreactor greatly limits the choice that can be utilized. In order to start the cracking process or the combustion of the chemical fuels, a resistive heater is needed over the reaction zone. Electrical connection to this heater is made through lead wires and contact pads which place several constraints on the packaging process.

For the current microreactor design, we require a bonding method that possesses the following characteristics in addition to the capability of forming a hermetic seal:

- high bond strength
- tolerant of surface roughness on the order of 0.5um due to the metallization
- compatibility with the process history of the device
- ability to prevent electrical shorting of the lead wires
- relatively simple to implement

The first constraint is to ensure that the packaged device will retain hermeticity during subsequent processing and handling. The second, third, and fourth constraints are imposed by the current microreactor design and fabrication steps. The fifth constraint is a general characteristic desired of MEMS packaging. The microreactor fabrication is rather complex, so a simple bonding method will increase packaging yields.

Once a compatible packaging method is chosen, a way of evaluating the level of vacuum achieved within the package is needed. There are several MEMS vacuum sensors that have been developed over the years. Common devices are diaphragm gauges, friction gauges, and thermoconductivity gauges. More abstract designs such as ion gauges or cold cathode gauges have been proposed but none have been implemented reliably [7]. A sensing mechanism that is accurate in the pressure range of interest, robust in design, reliable in performance, and simple in fabrication is desired.

2.2 – Bonding Techniques

Silicon fusion bonding is the process of joining two pieces of silicon through a surface preparation step, physical contact between the surfaces, and a high temperature anneal to strengthen the bond. The surfaces need to be clean and smooth to achieve hydration for a reliable bond. It has been noted that surfaces with a roughness greater than 1nm will generally fail to bond successfully, failing to meet the constraint on surface

roughness [2]. Additionally, the high temperature anneal at >800°C may be detrimental to the microreactor if there are materials with significant thermal mismatch.

Anodic bonding is the bonding of silicon to glass using strong electric fields and elevated temperatures of 300-400°C to create a chemical bond at the interface. The requirement on the cleanliness and smoothness of the surfaces to be anodically bonded is slightly more tolerant than that needed for silicon fusion bonding, but 0.5um greatly exceeds the limit [2]. The large voltages of 200-1000V needed to produce an anodic bond can be problematic. The large fields can potentially induce charging, resulting in damage to the device to be packaged.

Intermediate material bonding using glass frit or solder is a low temperature bonding technique that has excellent reflow characteristics, allowing for the bonding of rough surfaces. A relatively strong bond can be achieved at moderate temperatures and without the need for large voltages. This bonding method is a good choice since it readily meets the first three constraints listed above. Also, the freedom to choose a frit or solder with specific physical properties that are desired makes this technique quite versatile.

Glass frit was chosen over solder as the ideal material for two main reasons. A bond using solder has the potential to electrically short the connections to the resistive heater during the reflow process. Using an electrical insulator such as glass will satisfy the fourth constraint readily. Furthermore, the need to deposit a wetting metal prior to the solder complicates the fabrication process significantly. To prevent the wetting metal from shorting out the electrical connections, an insulating layer must be deposited beforehand. Avoiding the use of solder will keep the packaging scheme simple, satisfying the fifth constraint listed above.

Other forms of intermediate material bonding are gold thermocompression bonding and gold eutectic bonding. Thermocompression bonding relies on the plastic deformation of a clean and flat metallic surface, along with the simultaneous application of heat and pressure to produce a bond [6]. Gold is an excellent choice for the bonding metal since it is relatively soft and does not readily oxidize. In gold eutectic bonding, gold is deposited between silicon surfaces followed by the application of heat and pressure. Silicon diffuses into the gold until the interfaces form a eutectic alloy that bonds the surfaces. These methods of intermediate material bonding are not desirable for the same reasons that solder was not chosen over the glass frit.

Despite the advantages of using glass frit vacuum packaging for the micro-fuel processor systems in development, there is one major shortcoming - the technique is not one that is well established. Since there are many available glass frits to choose from, the development and optimization of a standardized glass frit vacuum packaging scheme is nonexistent. Significant work needs to be conducted to develop a successful vacuum packaging scheme that is compatible with the glass frit that is chosen.

2.3 – Vacuum Sensing

Diaphragm gauges utilize the deflection of a suspended membrane as the sensing mechanism. The pressure difference between the ambient and a reference pressure will cause the membrane to bend. The amount of bending can be determined by a capacitor configuration or a piezoresistive configuration. In the capacitor configuration, metal is deposited on one side of the membrane to serve as an electrode of a capacitor. The other electrode is placed parallel to the membrane and mechanical deflections will produce a change in the measured capacitance. In the piezoresistive configuration, piezoresistors are deposited along the edges of the membrane. The strain induced by the membrane deflection will produce a change in the measured resistance.

There are several issues with diaphragm gauges that are quite undesirable. Most notably is the strong dependence that the plate equation has on the thickness of the membrane. This makes the bending behavior extremely sensitive to fabrication irregularities. Additionally, the deposition of metal for the capacitor configuration adds a good deal of complexity to the fabrication steps while the use of piezoresistors is unreliable due to residual stresses.

Friction gauges utilizes a resonating structure such as a cantilever or comb driver to determine pressure. The device can be driven into resonance and the quality factor extracted. From the quality factor, one can determine the amount of damping in the system which provides information on the pressure of the system. The need for moving structures and the strong dependence the resonant frequency has on device dimensions make friction gauges undesirable.

Thermoconductivity gauges utilize the dependence that heat dissipation has on pressure. If a heating element sits on a thermally isolated structure, the primary heat transport mechanism will be through radiation and conduction through air. The thermoconductivity of air decreases with pressure, so the power dissipation of the heating element can be used to back out the pressure. A thermoconductivity gauge is desirable for the intended application since it is simple to fabricate, and it doesn't require moving structures. Furthermore, the similarity of the sensor design to the resistive heater on the reaction zone of the microreactor to be packaged makes a thermoconductivity gauge ideal.

Chapter 3
Bond Optimization

3.1 – Motivation and Approach

The scope of this project is to continue the development of a glass frit vacuum packaging technique. From the conclusions of the work done previously, the primary focus is to minimize or eliminate the formation of voids in the frit layer. It is speculated that the voids are the main cause for the failure in packaging since they serve as leakage pathways [8]. A literature search revealed that other researchers believe void formation is an issue that must be addressed when using glass frit to create a hermetic seal, and that fine control of the bonding conditions is needed to achieve a voidless bond [9-13].

Glass frit is a generic term for any form of glass powder. The properties of the glass frit are generally identical to the type of glass from which it is made. For handling purposes, these glass frits are usually mixed with an organic binder prior to use. Glass frit bonding is a type of intermediate material bonding that utilizes glass as glue. The first step is to deposit the glass frit onto one of the surfaces that is to be bonded. Organic binders and other impurities used to facilitate this deposition step should be removed before the bonding step. This is usually accomplished through a thermal process called pre-sintering that burns off the unwanted materials. Once this is accomplished, the bonding surfaces are brought into contact, compressed, and heated above the melting point of the frit. The glass powder melts, reflows, and forms a continuous layer of glass that bonds the surfaces once cooled.

The plan of action is to find a set of bonding conditions, covering pre-sintering parameters and bonding parameters, which will produce a voidless bond. Pre-sintering parameters comprise of the peak temperature used, the hold time at that temperature, the heating and cooling rates, and the ambient environment. Bonding parameters include the outgassing temperature, the outgassing time, the bonding temperature, the bonding time, the heating and cooling rates, and the amount of stainless steel weights used to induce an applied pressure. The material studied is GPR-10, a glass frit tape manufactured by Vitta Corporations, which has the properties given in Table 3-1.

Table 3-1. Physical Properties of GPR-10

Property	Value
Glass Family	Lead-Zinc-Borosilicate
Glass Type	Vitreous
Annealing Point	~ 425°C
Softening Point	~ 510°C
Working Temperature	552-600°C
Coefficient of Thermal Expansion	6.5 x 10^{-6} m/m°C
Dielectric Constant, 1 megacycle, 25°C	12

A logical starting point is to determine how the pre-sintering parameters will affect the bond quality when using the established bonding sequence. Once the pre-sintering process is well understood, attention can be given to the bonding parameters if needed. The proposed experimental methodology is to bond pieces of silicon that have been pre-sintered under various conditions to glass. Pyrex 7740 is utilized since it is thermally matched to silicon and its transparency permits the visual inspection of the bond layer.

3.2 – Pre-sintering Parameters

As mentioned above, pre-sintering is used to remove unwanted components in the glass frit prior to bonding. Being a glass frit tape, GPR-10 has organic binders and adhesives that should be burned off beforehand since the outgassing of these materials can potentially degrade the reliability of the bond. This thermal process can be carried out in a box furnace, a hot plate, or any other apparatus that can be used to effectively heat the glass frit. This section will discuss the steps taken to optimize the pre-sintering process. A box furnace was utilized for the air and inert environments, while a makeshift oven/hot plate was used in the vacuum ambient. The experimental conditions explored are summarized in Table 3-2 and images from this work are compiled in Appendix F.

Table 3-2. Presintering Trials

Trial	Set	Ramp Up	Peak Temp	Hold Time	Ramp Down	Ambient
1	A	90 min	520°C	30 min	120 min	Air
2	A	90 min	520°C	60 min	120 min	Air
3	A	90 min	520°C	120 min	120 min	Air
4	B	90 min	~500-540°C	30 min	~120 min	Vacuum
5	B	90 min	~500-540°C	60 min	~120 min	Vacuum
6	B	90 min	~500-540°C	120 min	~120 min	Vacuum
7	C	90 min	520°C	120 min	180 min	Inert (N_2)
8	D	90 min	300°C	30 min	180 min	Air
9	D	90 min	300°C	60 min	180 min	Air
10	E	30 min	450°C	60 min	180 min	Air
11	E	30 min	520°C	60 min	180 min	Air
12	E	30 min	500°C	60 min	180 min	Air
13	E	30 min	475°C	60 min	180 min	Air
14	E	30 min	490°C	60 min	180 min	Air
15	F	30 min	490°C	600 min	180 min	Air
16	F	30 min	450°C	600 min	180 min	Air
17	F	30 min	300°C	600 min	180 min	Air

The pre-sintering parameter used in the previous work was a hold at 500°C for 15 minutes in air. Using these conditions as a basis and speculating that the void formation was due to an incomplete burn-off of organics, the parameters defined as Set A in Table 3-2 were chosen. Under these conditions, the glass frit had reflowed and formed a brittle layer of glass with cracks. Longer hold time decreased the number of cracks in the "glaze" but increased the relative lengths of the cracks. The cracks are believed to stem from residual stresses in the glaze since extended hold times had an annealing effect. Additionally, it was observed that the glazing resulted in substantial surface roughness as shown in Figure 3-1. This is most likely due to the manner in which the glass frit melts and reflows.

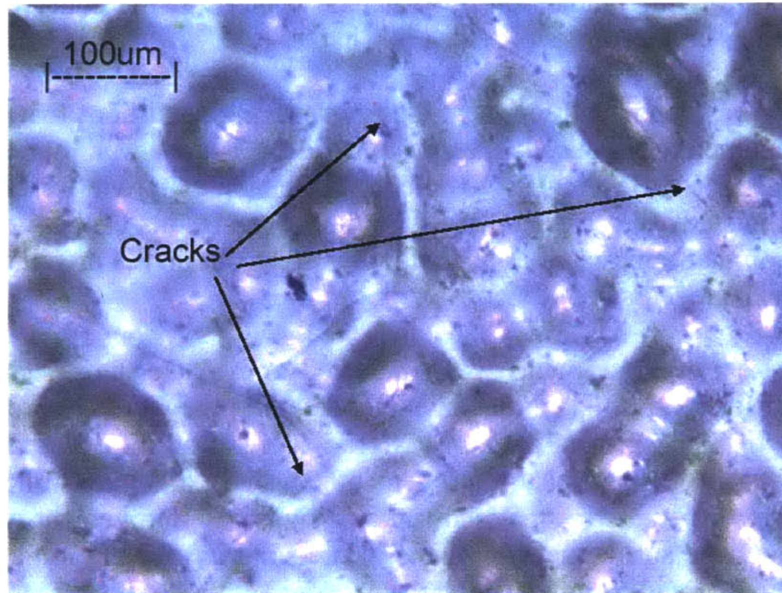

Figure 3-1. Rough Glazed Surface with Cracks

The pre-sintering conditions defined as Set B in Table 3-2 was chosen to evaluate the possibility of performing a pre-sinter and bond in one continuous step. This could potentially minimize the residual stresses and reduce the cracking that is evident from the results of Set A. The pre-sintering was carried out in the vacuum bonding apparatus developed in the work by Chou [8]. Samples were placed in the crevice of the heating chuck that is used for bonding. Since the chuck is designed to hold a stack of silicon dies, placing one die in this chuck essentially creates an oven/hot plate. The results of this experiment showed that the glass frit did not reflow at any of the hold times. The texture of these samples looked similar to that of un-sintered frit but the surface was charred and littered with burnt debris. Increased hold times resulted in increased charring, leading to the conclusion that vacuum pre-sintering does not effectively remove organics.

Set C was conducted in attempts to understand why the glass frit did not glaze over in Set B. Trial 3 was repeated in the box furnace but with a nitrogen flow to produce an inert environment. The extension in the ramp down time is an effort to

reduce the residual stresses of the pre-sinter process. The result of this experiment showed that the frit reflowed but exhibited burned particles across the surface. It was concluded that convection is needed for the glass to reflow and oxygen is needed to perform a clean burn-off. The experiments conducted so far limits the pre-sintering process to heating in air.

The parameters for Set D were chosen since the frit literature stated that a short ramp to 350°C with a 10-15 minute hold is sufficient to burn off the organic binders. The results of this experiment showed that the glass frit did not reflow and that the frit was unaffected by hold times. It was concluded that temperature is the critical parameter in the pre-sinter process. The bonding of Set D revealed that a temperature of 300°C is sufficient to burn off the binders but insufficient to burn off the adhesives. Additional information on this conclusion is provided in Chapter 6.

Trial 10 was conducted to repeat the pre-sintering conditions that Cha *et. al* used [9]. These parameters produced a very clean and pristine layer that did not reflow. Subsequent trials of Set E were used to determine the temperature in which the frit begins to reflows and to study the effects of the ramp rate. The results of these experiments led to the conclusion that ramp rate has an insignificant impact on the pre-sinter process, and the onset of glazing occurs at 500°C.

The last set of experiments was conducted to evaluate the effect that hold time had on the frit. It was speculated that an extended hold time would improve the burn-off but the results of Set F proved otherwise. Trial 15 resulted in a glazed surface, while Trial 17 did not show a significant improvement over the experiments of Set D. Trial 16 was the only set of parameters that showed any signs of improvement without glazing. Figure 3-2 shows the substantial difference in pre-sintering for the initial parameters of Trial 1 and the optimized parameters of Trial 16.

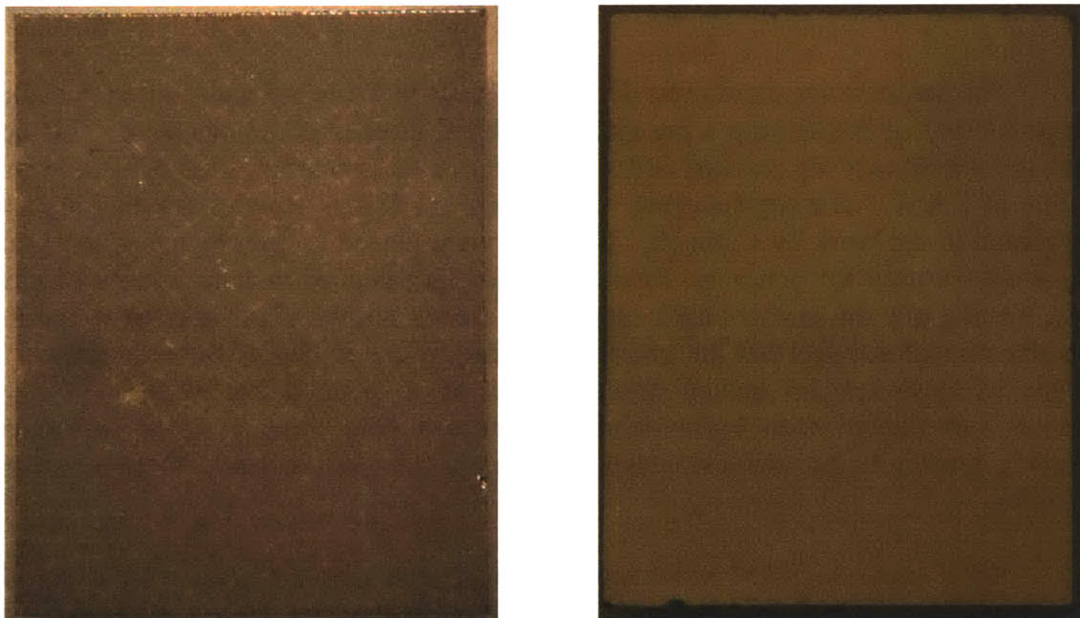

Figure 3-2. Comparison of Initial Pre-sinter and Optimized Pre-sinter

3.3 – Bonding Parameters

Several bonding parameter sets have been investigated and are summarized in Table 3-3. The outgassing step is a hold at an elevated temperature to drive out gases and water that might have absorbed in the frit during handling. The ramp to the outgassing temperature is not critical and the outgas time is fairly arbitrary. No ramps down times are included in the table because all the bonds were performed in a vacuum environment and allowed to cool through radiation. The temperature of the bond chuck drops at the acceptable rate of ~10°C per minute when the heaters are turned off. Images from the experiments discussed in this section are compiled in Appendix F.

Table 3-3. Bonding Parameter Sets

Set	First Ramp	Outgas Temp	Outgas Time	Second Ramp	Bond Temp	Bond Time	Weights
1	30 min	300°C	60 min	60 min	600°C	15 min	5kg
2	30 min	300°C	60 min	60 min	600°C	15 min	2kg
3	30 min	400°C	60 min	60 min	600°C	15 min	5kg
4	30 min	400°C	30 min	30 min	500°C	60 min	5kg
5	30 min	300°C	30 min	15 min	450°C	45 min	5kg
6	30 min	300°C	60 min	15 min	500°C	15 min	5kg
7	30 min	350°C	60 min	15 min	500°C	30 min	5kg

The first two sets of parameters explored were derived from the work by Chou [8]. Several pre-sintered samples were bonded using these two bonding sets and the results compared. It was observed that having more weights increased the size of the voids that formed within the frit layer but decreased their quantity. This result is most likely due to the "squeezing" of trapped gases during the bond, forcing small voids to conglomerate into larger voids. This "squeezing" is a positive result since larger, sparse voids serve as better barriers to leakage than small, widespread voids. It was concluded that increasing the applied pressure will improve the bond quality so all subsequent bonding parameters utilized 5kg of weights.

Ideally, the optimization of the bonding parameters should be conducted after the pre-sintering has been optimized. Due to time constraints, bonding optimization was performed in parallel with the pre-sintering optimization. As new information was learned from the pre-sintering experiments, modifications to the bonding parameters were made and evaluated. Knowledge that the frit did not reflow at 450°C prompted the increase in the outgassing temperature of bonding Set 3. This change would potentially improve the bond since it will drive out absorbed gases and water vapor more effectively. No significant improvements in the bond were noticed with this modification.

When the frit reflow temperature was identified at 500°C, bonding Set 4 was proposed. The outgas time was decreased since the outgassing step did not appear to have a significant effect on the bond quality. The bonding temperature was reduced and the bond time extended. This was in hopes that a well controlled reflow would produce a better bond. The second ramp down was decreased to maintain a ramp rate of 200°C per hour. The results of this experiment showed a bond with a similar quality of that from Set 3. It is reasoned that the void formation mechanism is a function of total heat flux. A bond at higher temperatures and moderate hold times produce similar results of moderate temperatures and extended hold times.

Utilizing the results of Set 4, parameter Set 5 was proposed which attempted to decrease the total amount of heat flux to the sample. The times and temperatures of each step in the bond sequence was decreased. The result of this parameter set was a complete failure to bond. Bonding Set 6 increased the outgassing time, decreased the bond time, and used the reflow temperature of the frit as the bond temperature. The result of this experiment was a very weak bond that could be separated easily with a razor blade. The modification made for bonding parameter Set 7 resulted in a successful bond with no visible voids. The positive results of this parameter set led to the conclusion that the bonding has been optimized.

A simple experiment was conducted to provide a reference for how a good bond interface should appear. Samples that have been optimally pre-sintered were placed in a box furnace with a piece of Pyrex over the frit. The stack was heated to 520°C and held for 60 minutes with no applied pressure. The natural reflow of the glass frit will wet the Pyrex and form the bonded areas that appear as the dark regions in Figure 3-3. Parameter Set 7 produced a bond with no light regions indicating a voidless bond and supporting the conclusion made above.

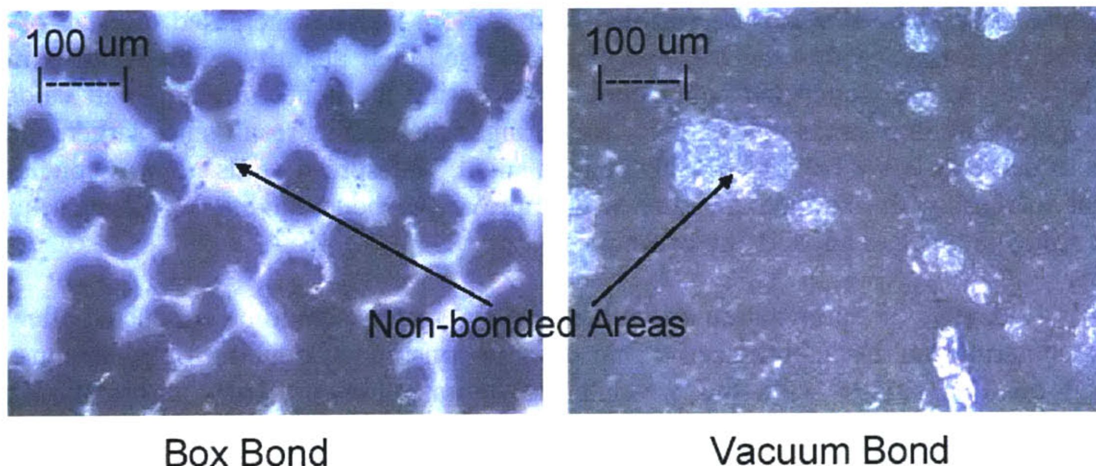

Figure 3-3. Visualization of a Good Bond

3.4 – Results

The work discussed in this chapter led to the successful optimization of pre-sintering and bonding parameters. Figure 3-4 highlights the advances made in the reduction of void formation in the frit layer during bonding. An optimization methodology has been established and utilized to significantly improve the quality of a glass frit bond. The major conclusions of this chapter can be summarized in the following list:

- an ideal pre-sinter should produce a clean burn off all organics without causing the frit to reflow
- crucial pre-sintering parameters are temperature followed by hold time
- oxygen is needed in the ambient to effectively burn off organics and adhesives
- void formation is a function of total heat flux delivered
- increased applied pressures improves bond quality

This list should be kept in mind for other glass frits that require optimization.

(a) Previous Bond Quality

(b) Optimized Bond Quality

Figure 3-4. Results of Bond Optimization

Chapter 4
Two-Step Approach

4.1 – Motivation

Utilizing the optimized pre-sintering and bonding conditions described in Chapter 3, several devices were packaged using the packaging scheme described by Chou [8]. Despite failing to produce a vacuum package, the optimized bonding achieved a seal that exhibited a slow leakage. The high pressure measured within the package is believed to stem from the outgassing of the frit and the interior surfaces of the cavity during bonding. A device that was packaged in two steps verified this assumption by producing a leaky vacuum package with an initial vacuum of <150mTorr. Exact details of these experiments are giving in Chapter 6.

The low pressure package achieved in the work described above is not readily reproducible, indicating that there is a need to overcome the issue of outgassing. Among the limited literature involving glass frit, a predominant application is the vacuum packaging of display panels [9-14]. Glass caps are initially bonded to the device utilizing a frit ring that is reflowed at elevated temperatures. The package is then pumped down through a tube and is sealed off with a tip-off as shown in Figure 4-1. Due to the similarities in this technology and what would like to be accomplished, an alternate packaging method was conceived that utilized an analogous two-step process.

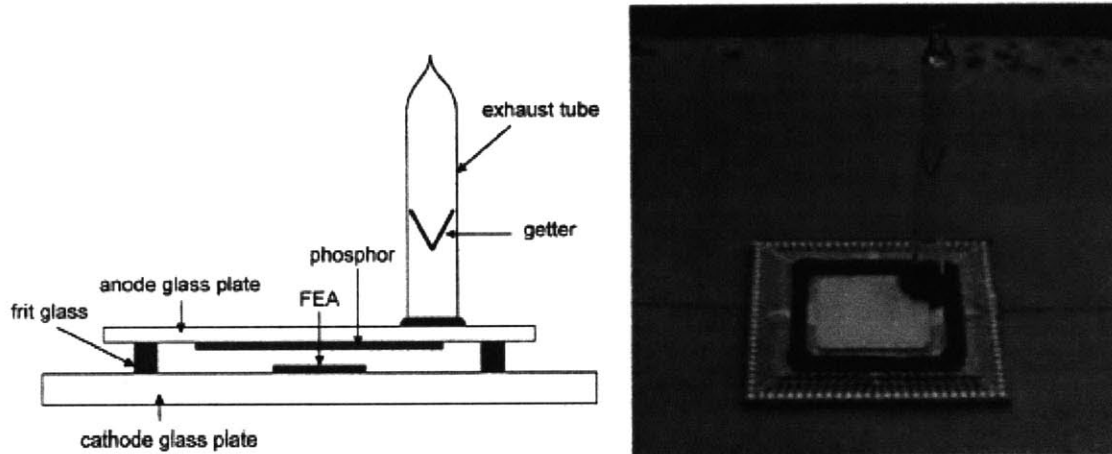

Figure 4-1. Schematic Diagram and Picture of a Packaged FED Panel [14]

4.2 – Packaging Concept

The proposed packaging concept is portrayed in Figure 4-2. The first step is the bonding of the caps to the device. The second step is the placement of the solder or glass

frit in the pump out holes. The final step is the melting of the solder or glass frit in a vacuum environment to seal the package. Bonding in the first step is to be conducted in a box furnace at atmosphere due to the improved temperature control of the furnace. The temperature controller of the vacuum bonding apparatus does an extremely poor job at maintaining the system temperature at the desired set-point, potentially introducing cracks from unwanted thermal stresses.

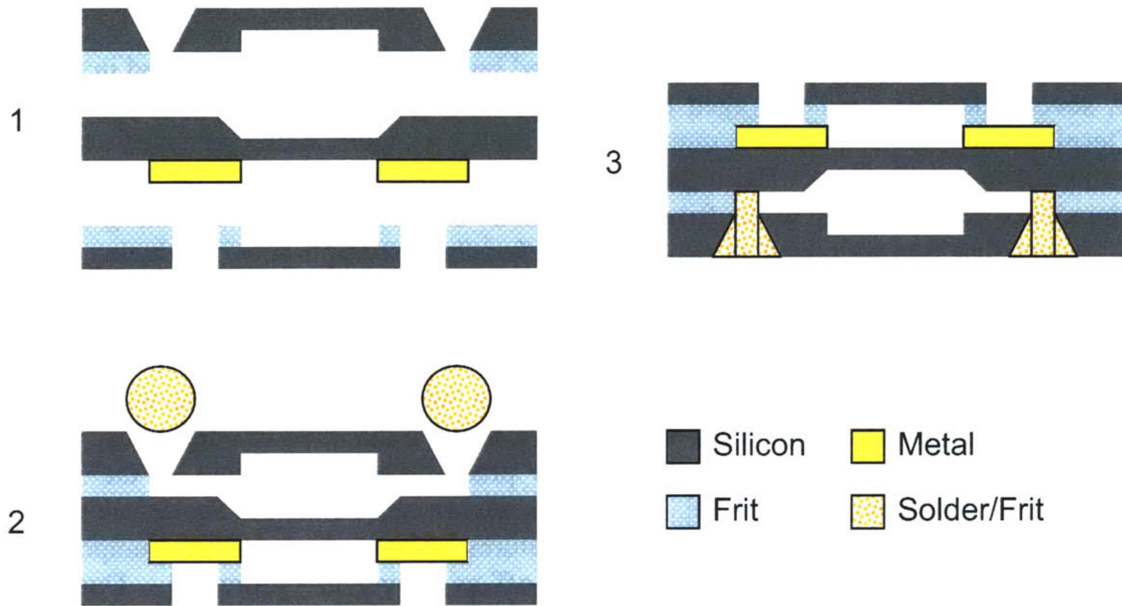

Figure 4-2. Schematic for Two-Step Process

Challenges in developing this concept are the cap design, and the material choice for the final seal off. These two issues will be addressed individually in the following sections of this chapter. The optimization of the box furnace bonding can be readily accomplished by using the methodology prescribed in Chapter 3. Experimental results of this packaging scheme will be discussed in Chapter 6.

4.3 – Cap Design

Designing appropriate capping dies for the proposed two-step process is the first objective. Since the test structure in the previous work is to be used, the capping dies must be designed to accommodate the features of the device. Additionally, the final package is expected to be able to incorporate getters. Getters are highly reactive alloys that will be used to maintain the vacuum level within the packaging. They function as micro-pumps by absorbing any gases that outgas from the interior surfaces of the package. Detailed information on the getter St122 is given in Appendix B. The proposed design for the bottom cap is shown in Figure 4-3. Designs for a top cap will not be addressed since the one used in previous work is suitable for the new packaging scheme.

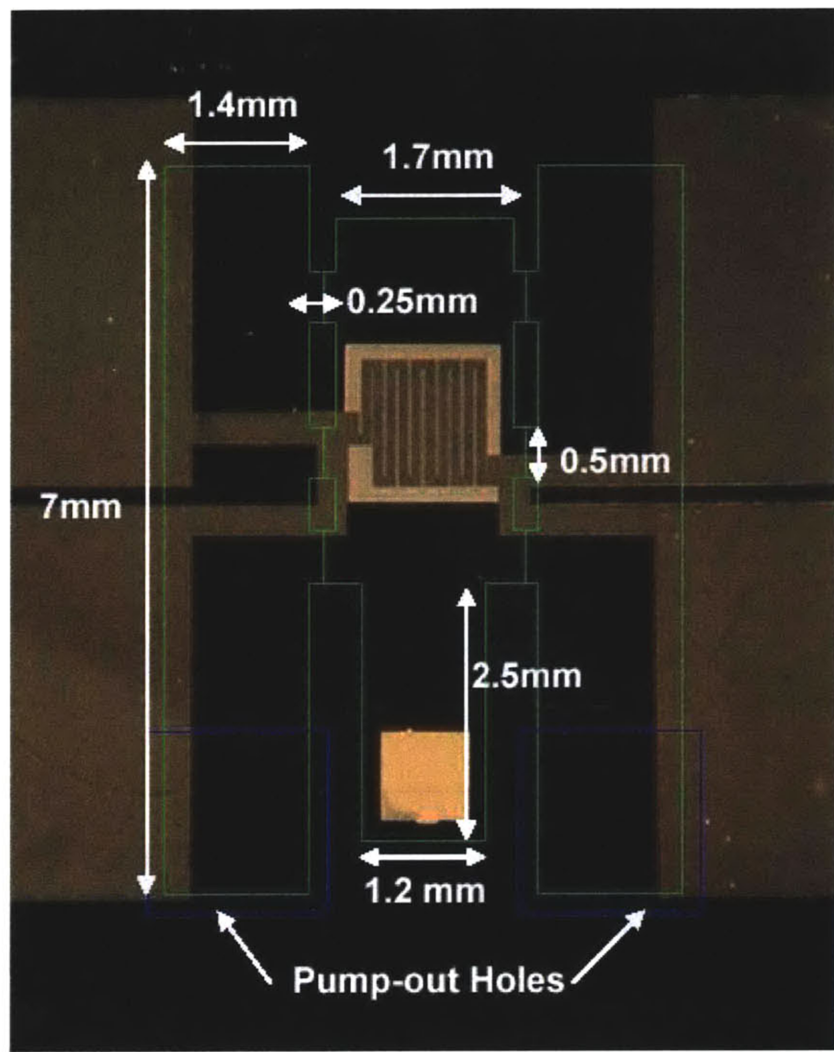

Figure 4-3. Design of Bottom Cap

The pump-out holes are designed with the intention of etching by KOH. The sloped sidewalls associated with KOH are desired due to concerns with wetting of the final seal-off materials. These holes are designed large enough for the insertion of getters because incorporating getters prior to bonding is impractical. Heating the getters before achieving a vacuum seal will activate the getters and cause them to saturate, rendering them useless. The dual trench design used facilitates the insertion of getters and can accommodate 10-12 getters per trench. Rectangular pillars are placed around the membrane to confine the getters in the trenches. This prevents the getters from shifting around and potentially destroying the device.

Two new designs are proposed along with the original dual trench design. As can be seen from Figure 4-4, the designs are all very similar except for the geometry of the pump-out holes. Design (a) is the original concept with a pump-out hole in the shape of a

funnel. Design (b) introduces an undercut in order to create a stop valve. This design can be utilized if the seal-off material significantly wets into the trenches. Design (c) removes all vertical sidewalls from the pump-out hole. This design can be utilized if the seal-off materials have issues with wetting and adhesion. The square corresponding to the KOH hard mask is calculated to be 1.8mm per side for designs (a) and (b), and 2.1mm per side for design (c). These calculations were made assuming the narrowest region of the pump-out holes should be kept at a minimum of 1.4mm and the wafer to be used will have a <100> crystal orientation.

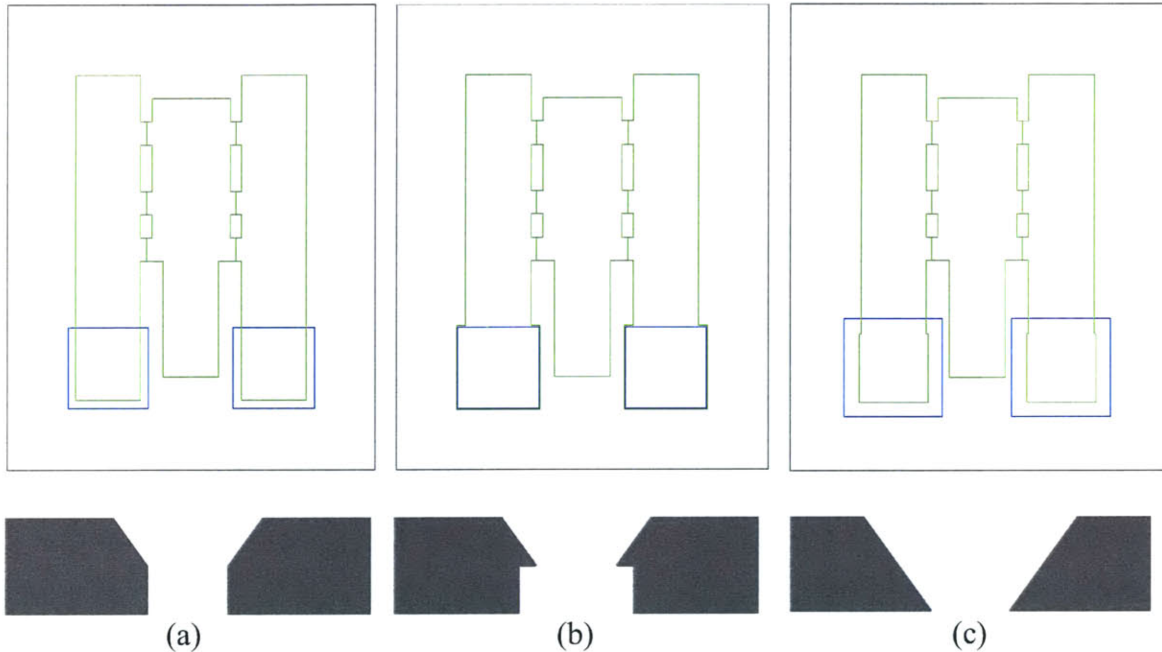

Figure 4-4. Three Different Cap Designs

4.4 – Final Seal-Off

Several constraints were kept in mind when searching for a final seal-off material. The most important criterion is a working temperature in the range of 300-500°C. This range is defined by a practical getter activation temperature and the reflow temperature of GPR-10. The second constraint is a material that will not outgas during the seal-off process. The outgassing issue was the reason this new packaging scheme was developed. Finally, a good thermal match to silicon is desired to minimize stresses that can be detrimental to the seal.

The search for a solder brought about a few additional constraints to those mentioned above. Solders and their associated wetting metals typically develop a native oxide that can degrade the quality of the bond. In general, a flux is used to remove the oxide but this can be deleterious to the packaging scheme. Flux is a corrosive fluid that will most likely wet into the trenches of the cap and potentially damage the device that is being packaged. Additionally, the flux may present itself as a source of outgassing. It

was determined that gold-based solders would be ideal since they do not require the use of flux. Potential issues with using these solders are the formation of a gold-silicon eutectic at 363°C and the material costs.

Low melting glass is a simple and cost-effective alternative to gold-based solders. Using glass would eliminate the need to deposit wetting metals on the packaged device. A product search revealed that most low temperature glasses have working temperatures out of the desired range. Furthermore, those with low enough melting points have a significant thermal mismatch to silicon. It was determined that solder glasses or glass frits were the only type of glass that met most of the constraints. Outgassing of the frit is still a potential issue, but the investigation of these materials can be worthwhile due to the significant reduction in costs. The materials that were found to be compatible are summarized in Table 4-1.

Table 4-1. Physical Properties of Seal-Off Materials

Materials	**Sealing Range**	**Liquidus**	**Solidus**	**CTE**	**Density**
DM2700PF	320-375°C	N/A	N/A	7.7 ppm/°C	7.6 g/cc
DM2760PF	380-450°C	N/A	N/A	6.9 ppm/°C	7.0 g/cc
B-10105	450-480°C	N/A	N/A	5.4 ppm/°C	-
B-10127	430-470°C	N/A	N/A	4-5 ppm/°C	-
75Au/25In	N/A	465°C	451°C	-	13.7 g/cc
82Au/18In	N/A	485°C	451°C	-	14.9 g/cc

Chapter 5
Device and Fabrication

5.1 – Device Overview

The overall packaged test structure has a general schematic shown in Figure 5-1. There are three main components, a top cap, a bottom cap, and a device layer. The top cap consists of a shallow trench and through holes. The trench is to prevent physical contact of the heating resistor with the cap during bonding, and the through holes provide access to the contact pads of the device layer. The bottom cap is quite simple and only has a deep trench for the purpose of holding getters. The device layer is the most complex and comprises of a metal resistor sitting on a nitride membrane and a pressure equilibration hole. The resistor is the sensing element and the equilibration hole is to ensure that the entire sealed cavity is at the same pressure. Additional details of the design shown in Figure 5-1 are given in the work by Chou [8]. The rest of this chapter discusses the fabrication steps of the process flows provided in Appendix C.

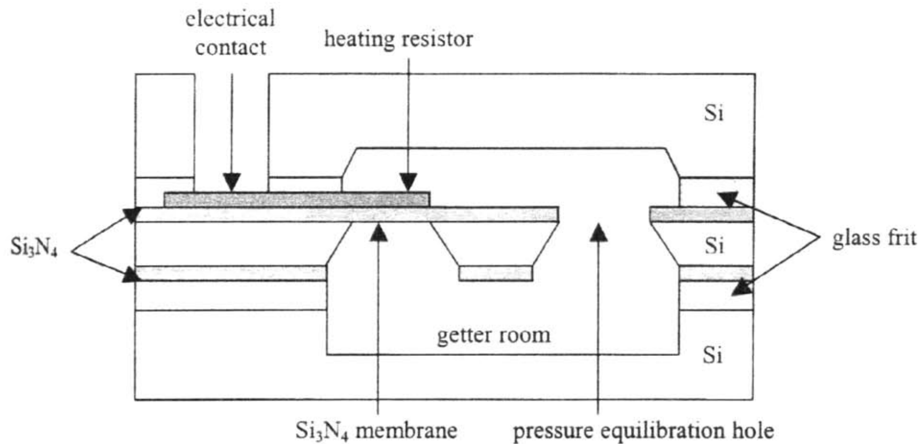

Figure 5-1. Overall Packaged Device Schematic [8]

5.2 – Capping Dies

The main fabrication steps for the top and bottom cap are outlined in Figure 5-2. For the top cap, the first step is to grow thermal oxide in a diffusion tube. Next, thin photoresist is spin coated and patterned to serve as a mask for an oxide wet etch. The flipside of the wafer is painted with thin resist to prevent the flipside oxide from being etched during the BOE. The wafer is then target mounted to a quartz handle wafer and dry etched for ~15um using DRIE. After the dry etch, the wafer is dismounted from the handle wafer and cleaned. Similar steps are repeated to pattern the oxide on the backside of the wafer. To prevent resist from burning during long etches in the DRIE tool, the

flipside must be cleaned to ensure good thermal contact to the handle wafer. The cleaning step will remove the patterned resist so photolithography is repeated but with some modifications. Thick resist is used to survive the long etch times and the new exposure needs to be aligned to the previous wet etch. The wafer is then mounted, etched through, dismounted, cleaned, and stripped of oxide.

The fabrication of the bottom cap is quite similar to that for the top cap. Thermal oxide is grown and patterned using the same sequence of steps as for the top cap. Once again, good thermal contact to the handle wafer is required so the wafer is cleaned and photolithography is repeated with thick resist. The wafer is mounted, etched for ~250um, dismounted, cleaned, and stripped of oxide.

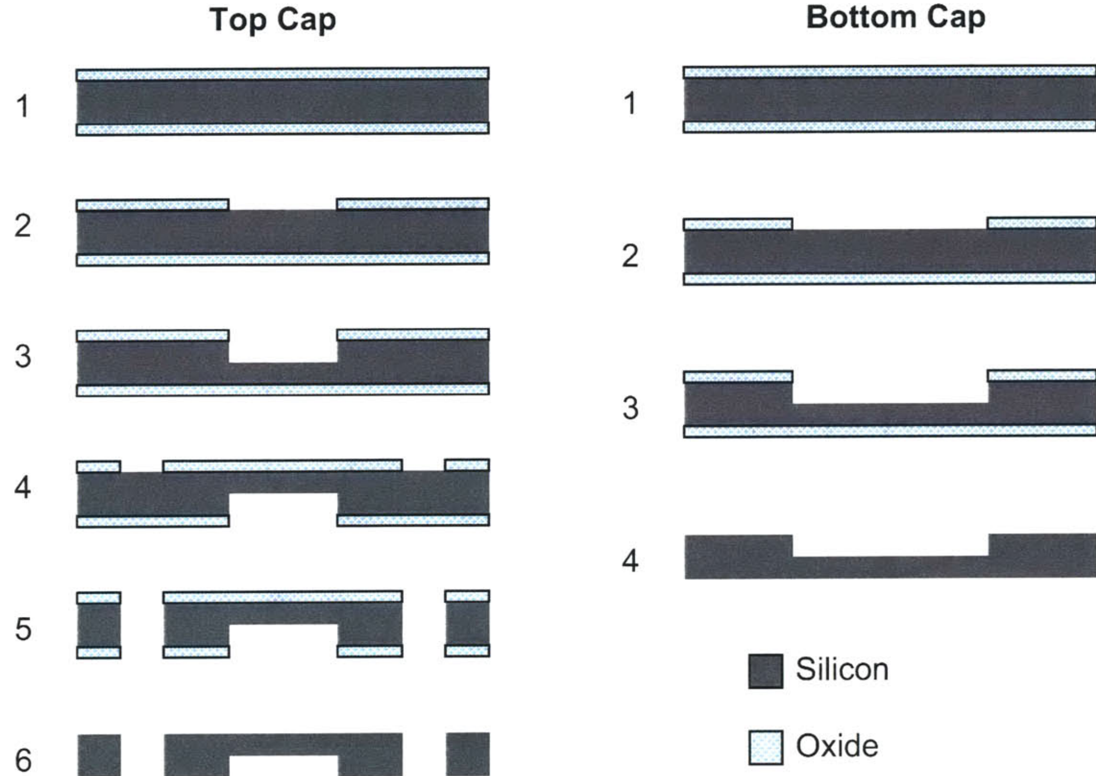

Figure 5-2. Fabrication Steps for the Top and Bottom Caps

5.3 – Device Layer

The fabrication steps for the device layer are shown in Figure 5-3. Low stress nitride is deposited to simultaneously serve as the thermally isolated membrane and as the KOH hard mask for the backside. The backside is patterned using thin resist followed by a dry etch. The wafer is cleaned, and then image reversal resist is used to define the heating element on the frontside. A sandwich layer of Ta/Pt/Ta is deposited via e-beam followed by a lift-off process. The wafer is then etched with KOH to create the nitride membrane and the pressure equilibration hole. Since platinum etches in KOH, a one-

sided Teflon chuck is used to protect the metallization. A subsequent anneal is used to strengthen the metal and to reduce thermal drift during sensing. A critical step is to spray-coat photoresist over the wafer prior to dicing. The membranes are extremely fragile and will break in the die-saw tool if uncoated. Once the devices have been diced, the dies need to be cleaned of resist, and the nitride membrane over the pressure equilibration hole needs to be broken manually.

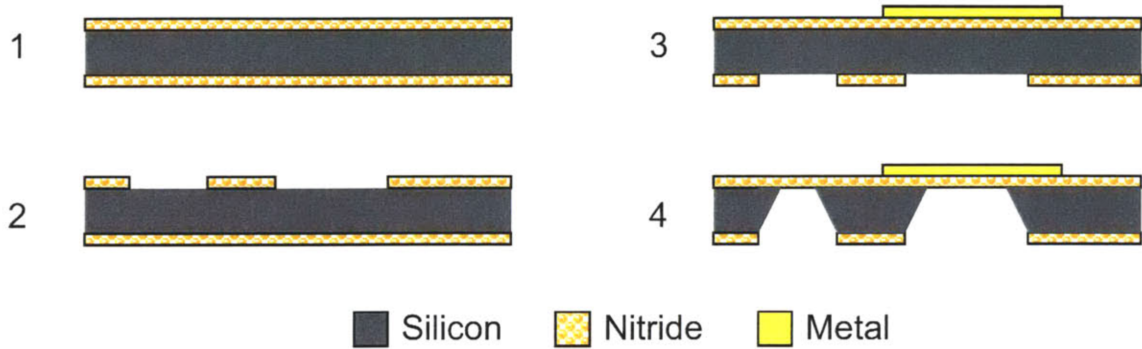

Figure 5-3. Fabrication Steps for the Device Layer

5.4 – Two-Step Bond Cap

Fabrication of the two-step bond cap is portrayed in Figure 5-4. Initially, low stress nitride is deposited to serves as a KOH hard mask. The nitride is patterned in a similar fashion as for the device layer. The wafer is then immersed in KOH for a fixed time to leave ~25-50um of silicon in the through holes. This step is important for the successful patterning of the backside. Next, the nitride is stripped and a thermal oxide is grown. The subsequent steps are identical to that for the bottom cap described above.

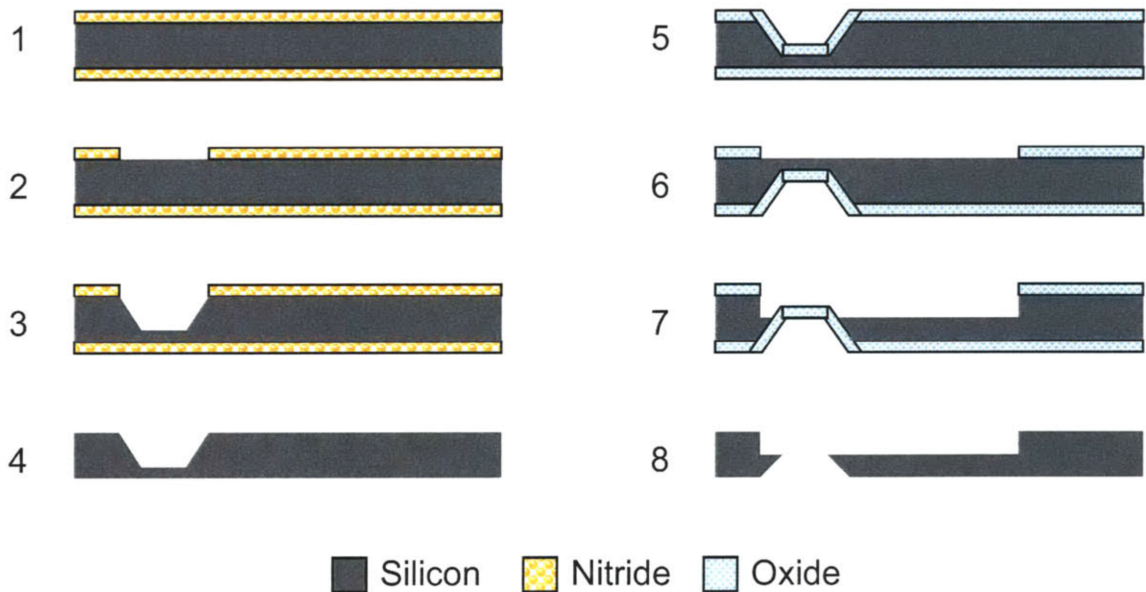

Figure 5-4. Fabrication Steps for Two-Step Bond Cap

Chapter 6
Experimentation

6.1 - Calibration

Calibration of the test structure is performed to determine how well the fabricated test structure performs compared to the analytical model developed and is discussed in Appendix A. Assuming a constant temperature operation of the thermoconductivity pressure sensor, power dissipation at the target temperature is recorded as a function of pressure. This calibration curve serves as a method to determine the level of vacuum achieved in the packaging schemes evaluated.

Calibration curves were generated utilizing the custom made four-point probe chuck shown in Figure 6-1. A HP-E3612A is used to supply a current, while a Keithley 179 TRMS Multimeter measures the voltage drop across the resistor. After taking an initial reading for the base resistance of the device using a very small current, a target resistance that corresponds to 87°C is calculated assuming a TCR of 0.38% for the platinum resistor. The probe chuck is placed in a vacuum chamber and held at a constant pressure through the use of a leak valve. The current is adjusted until the device produces a steady resistance close to the calculated target value. The pressure, current, and voltage is recorded where I×V will be the power dissipation at the recorded pressure. Data points for pressures between 30-1000mTorr are collected and plotted.

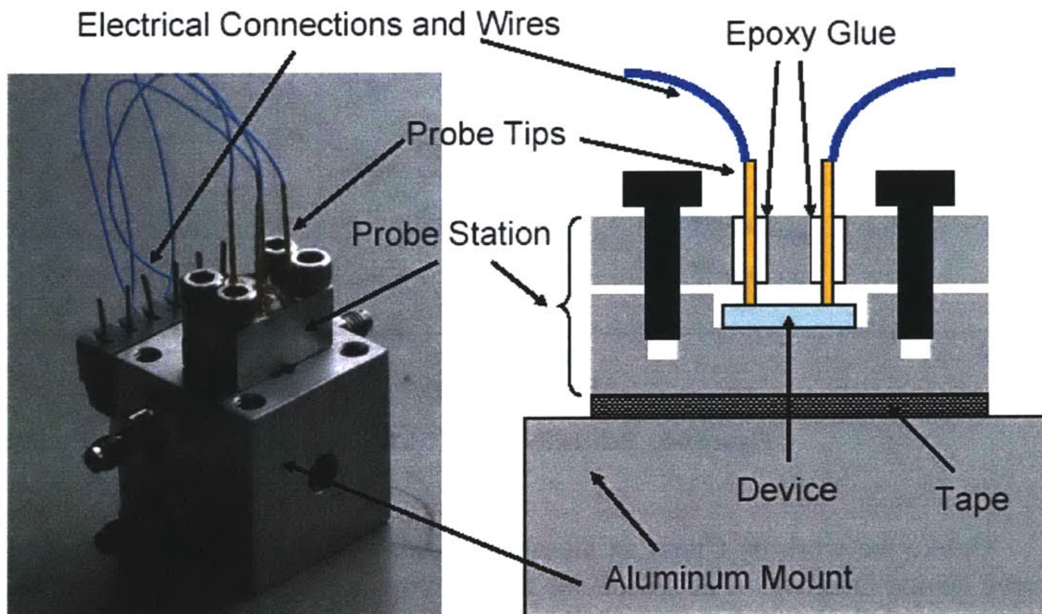

Figure 6-1. Four-point Probe Chuck
(The ports on the aluminum mount are from a previous experimental setup and serve no purpose here. The mount is used to facilitate handling of the probe station and to make electrical connections sturdier.)

An experiment was conducted to determine if the vacuum bonding process affected the performance of the sensor. The results of this experiment will establish the reliability of the test structure and determine if the sensor can be used to accurately determine the pressure in the package. A calibrated device is bonded with packaging caps that were deliberately made leaky, and then recalibrated. A similar process was repeated for devices that were bonded in an optimized box bond as part of the two-step bond process. The data from these experiments are shown in Figure 6-2. It can be seen that the curves line up quite nicely and is within our expected experimental error. This led to the conclusion that the optimized bonding processes do not have an effect on the device performance.

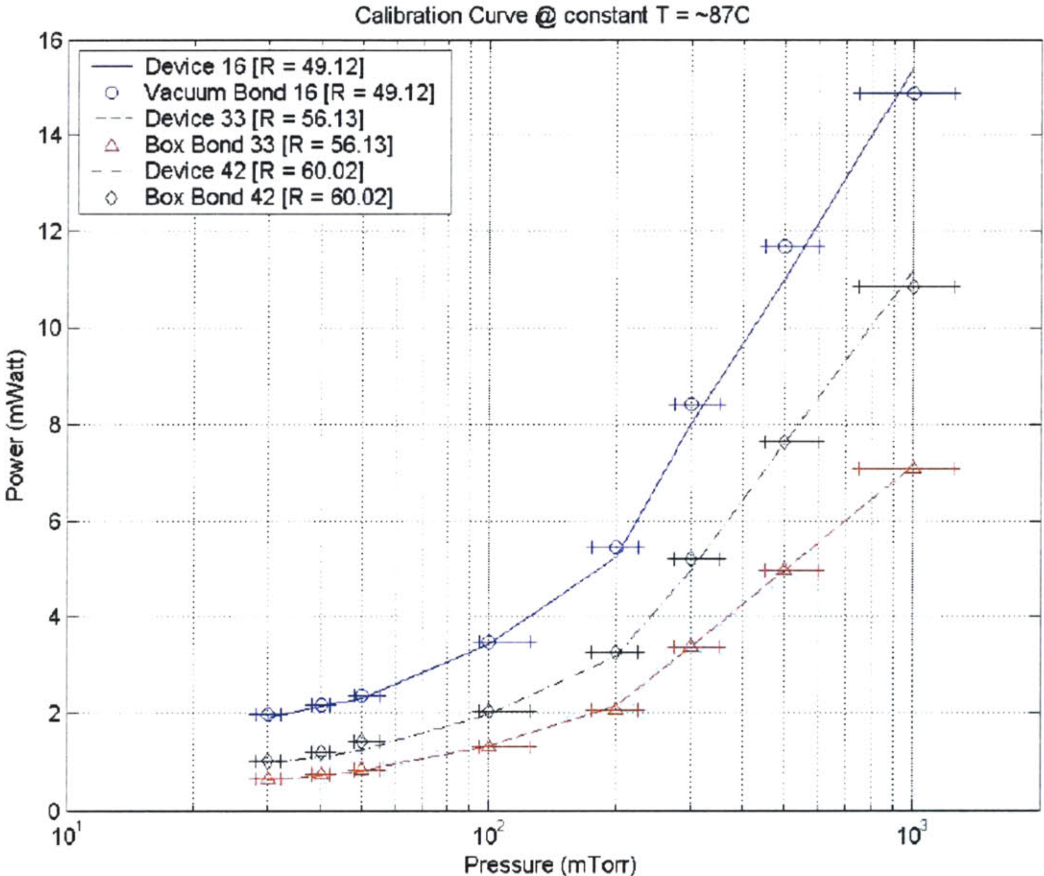

Figure 6-2. Reliability Test of Glass Frit Bonds

Unlike the work by Chou, an aluminum-oxide diffusion barrier is not needed to preserve device integrity. The reason for this difference is most likely attributed to the optimization of the bond processes. Chou speculated that the observed rise in device resistance is due to silicon diffusion from the glass frit into the metal line, forming a non-conductive platinum silicide [8]. Results of the current work indicate that this speculation is incorrect since glass frit has been placed directly over the metallization

without causing a change in device performance. Since bond optimization succeeded in the elimination of voids, the rise in device resistance observed by Chou can be due to metal fracture induced by void formation. The aluminum-oxide barrier utilized by Chou could have shielded the metallization from the damaging effects of the voids.

The sensor reliability experiment was repeated for packaged devices of the two-step bond process that went through an e-beam deposition of solder wetting metals. This was conducted to verify the reliability of the sensor after being processed post-bonding. Figure 6-3 shows the results of three different metal depositions. A slight increase in the power dissipation is consistent between all three devices. This is an indication that there are some changes in the heat conduction pathways that results from the e-beam process. These changes can stem from the heating that arises from the bombardment of energetic particles, and/or the exposure to a high vacuum that is in the microTorr range. Despite the slight increases, the devices still align quite well with the initial calibrations. It can be concluded that the sensors can still be used to indicate a vacuum package of at least 200mTorr.

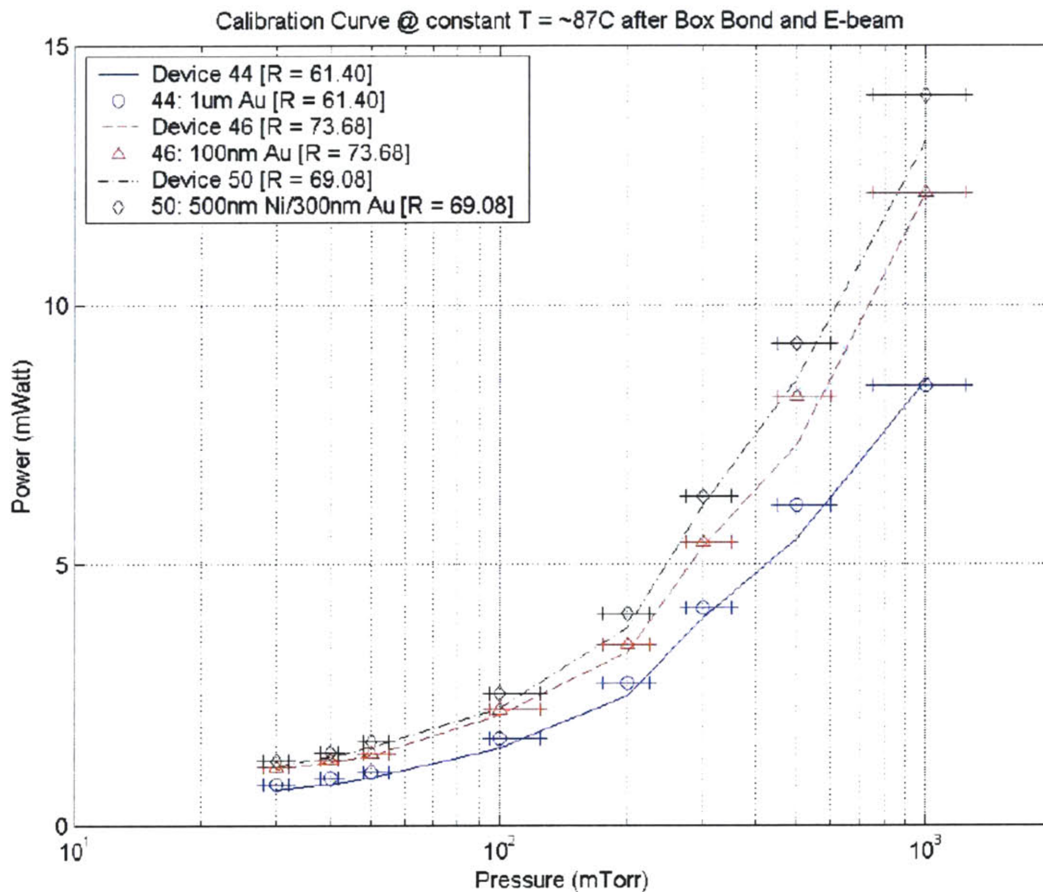

Figure 6-3. Reliability Test of Sensor After E-beam

Comparison of the various calibration curves of Figures 6-2 and 6-3 reveals that some devices demonstrate similar power dissipations for very different target resistances

while others have significant differences in power dissipation for similar target resistance. Ideally, if every test structure was identical, all the calibration curves would align, thus requiring only one calibration to be made. Due to non-uniformities in fabrication, and inaccuracies in determining the base resistance, calibration curves need to be generated for every device packaged.

A potential source of performance discrepancies can be traced to the KOH etch step. Discoloration in the metallization was observed after the device wafer was removed from the one-sided chuck. Since platinum is reactive with KOH, it is deduced that the Teflon chuck did not effectively protect the covered surface. Changes in metallization thickness can have a considerable impact on the heat conduction pathways. A more significant source of the inconsistencies observed may be due to the precision of the current source. Since very small currents are utilized to determine the base resistance of the device, on the order of the uncertainties of the power supply, substantial error can arise when the target resistance is calculated. If the measured base resistance if far from the actual base resistance, the calculated target resistance can correspond to a different temperature than 87°C. Variation in the operating temperature of the test structures will have noticeably different power dissipations.

6.2 – Frit Transfer

An important process in this experimental work is the placement of frit on the capping dies. In the optimization work, the frit was simply taped over the rectangular dies, compressed with a rubber stop to enhance adhesion, and the excess frit at the edges was removed with a razor blade. All surfaces that were covered with glass frit were cleaned with acetone and DI water beforehand. Placement of the frit on patterned structures such as the capping dies requires a little more finesse.

Frit transfer to the bottoms caps utilize a similar process to the one described above. The only difference is that care must be taken when performing the compression step. Pressing too hard can cause the frit to stick to the bottom of shallow features which is not desired. Because all the features of the bottom caps are quite deep, there won't be a significant problem if moderate force is used. After the bottoms caps are pre-sintered, the frit over the deep features can be easily removed by blowing with compressed air.

The top cap is where a problem with frit transfer was encountered. Since the shallow trench has a depth that is less than the thickness of the frit, there is no way to prevent the frit from getting in the trench if the conventional method is used. Scratching the frit off after pre-sintering is too labor intensive and there is little chance that a clean surface can be achieved. The technique displayed in Figure 6-4 was developed to overcome this issue.

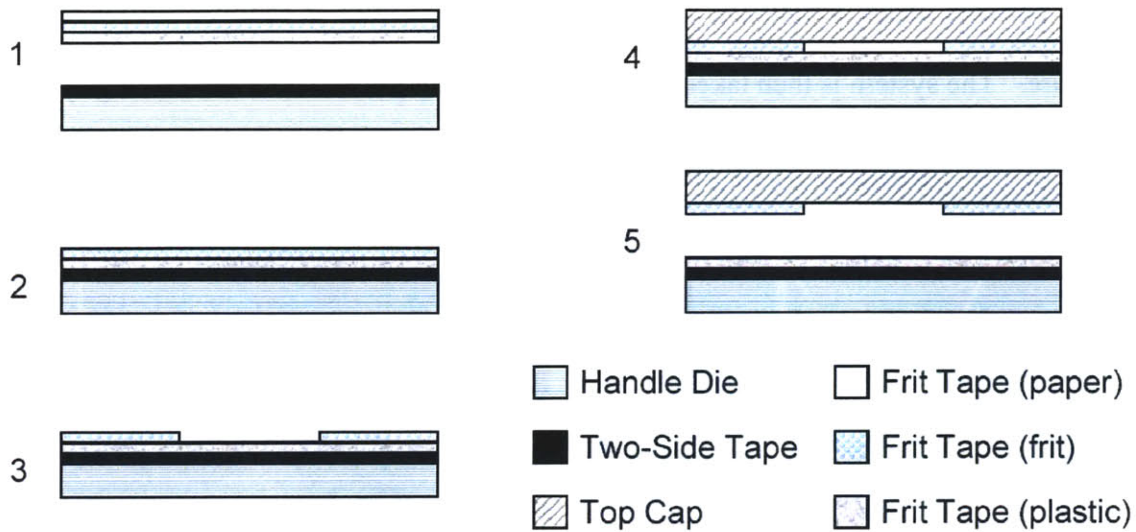

Figure 6-4. Frit Transfer Methodology

The glass frit tape comes as a sandwich structure that is comprised of a paper layer, the frit itself, and a plastic layer. The paper layer covers the adhesive side of the frit, while the top plastic layer is used to protect the frit. The frit transfer method was devised utilizing this information. Initially, double sided tape is placed on a handle die that is the same size as the capping die. The glass frit tape is then placed on the handle die with paper side up. Excess frit tape is trimmed off with a scissor and the paper layer is carefully removed with a razor to expose the adhesive side of the frit. A sharp knife is then used to manually cut out the frit from undesired areas. Once the frit has been crafted into the desired shape, the top cap is aligned and pressed onto the adhesive. After a subsequent pressing with a rubber stop, the frit layer readily separates from the plastic protection layer and transfers to the top cap.

6.3 – Vacuum Bonding

6.3.1 – Setup

The experimental setup used for vacuum bonding is shown in Figure 6-5. This apparatus can be separated into vacuum system components and bonding system components. The vacuum system comprises of a bell jar (BJ12X18) with a L-shaped gasket (LG12V), an electrical feed through color (FTC-12-1-8-O), a base plate (BASEPLATE12), a roughing pump (Trivac B D25B), a vacuum gauge (KJL205 and KJL6000), and a nitrogen backfill line with a leak valve. The bonding system comprises of cartridge heaters (CSH-101100/120) that are placed into a custom-made stainless steel chuck. The heating is managed by a temperature controller (CNi32 Series) that regulates the power from a variable AC supply with the help of a solid state relay (SSR240DC25), and a thermocouple (Type K). The pieces to be bonded are carefully aligned and placed

in the bonding chuck within the vacuum system. The chuck is sandwiched by ceramic insulators for thermal isolation, and weights are balanced on top to induce an applied pressure. The system is then taken through the bonding process with the heating system.

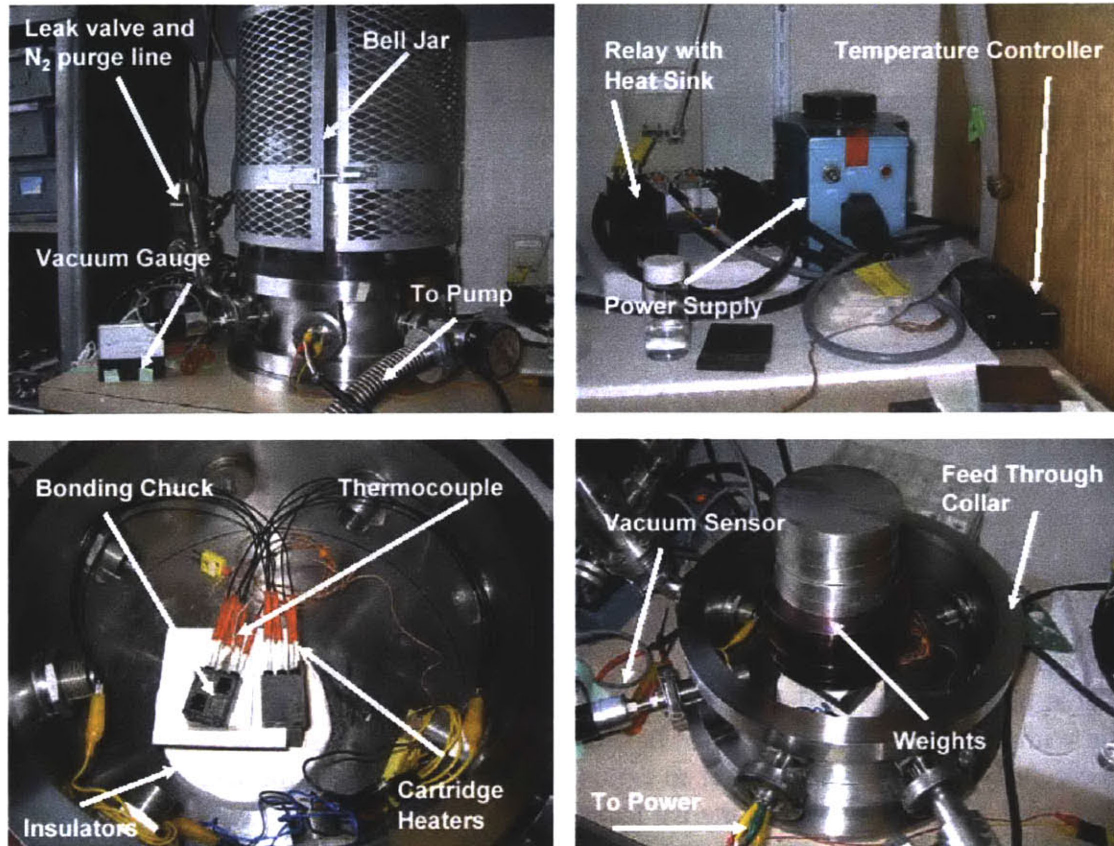

Figure 6-5. Vacuum Bond Setup

A significant issue developed with the original heaters during the bond process. It was observed that the electrical leads would melt off the heating sheath during rapid temperature ramps. It was determined that the stainless steel chuck was a poor heat sink for the heaters, causing the heaters to reach a much higher temperature than the rated value. New high temperature heaters (E1E43-AJ-12T) from Watlow were ordered that had ceramic beading over stainless steel leads. Additionally, a new copper bonding chuck was designed to serve as a better heat sink and allow for improved die alignment. Oxidation concerns are alleviated since the heating is performed in vacuum. The new components are shown in Figure 6-6 and the chuck dimensions are provided in Appendix E. A problem with the new chuck was that the applied pressures used caused the packaged devices to stick to the soft copper surfaces. This problem was resolved by utilizing buffer layers of silicon during the bond process.

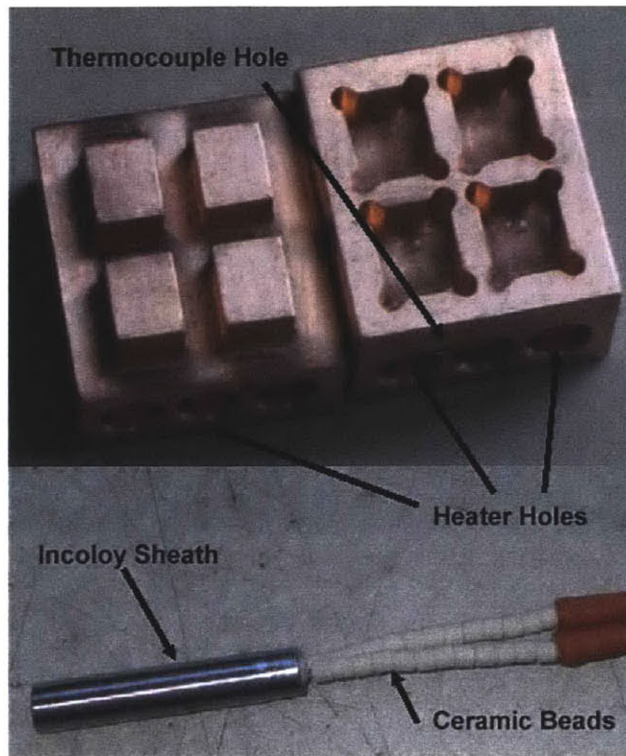

Figure 6-6. New Chuck and Cartridge Heaters

6.3.2 – Results

As mentioned in Chapter 3, bonding the pre-sintered samples of Set D led to the conclusion that a temperature of 300°C was insufficient to burn off the adhesives in the glass frit. Bonding these samples with the parameters defined as Set 1 in Table 3-3 produced a smooth, black interface between the Pyrex and silicon. Initially, it was speculated that the glass frit had formed a clear, voidless layer, and that the interface observed was the surface of silicon. Assuming the pre-sintering parameters and bonding parameters were optimized, several devices were bonded but no vacuum package was achieved.

In an attempt to visually determine if leakage pathways formed when bonding to a device, a piece of Pyrex was pre-sintered at 300°C and utilized as a cap. This experiment revealed that the preliminary speculations were wrong. The smooth, black surface was not that of a clean, voidless interface, but that of burnt adhesives from the frit. As can be seen in Figure 6-7, the frit did not become a transparent layer since the color of the nitride did not show through. From this, it was concluded that a temperature of 300°C and hold times of 30 minute and 60 minutes are insufficient to burn-off the adhesives in the glass frit tape. A positive observation made was that pre-sintered samples that did not glaze produce a bond with significantly smaller voids.

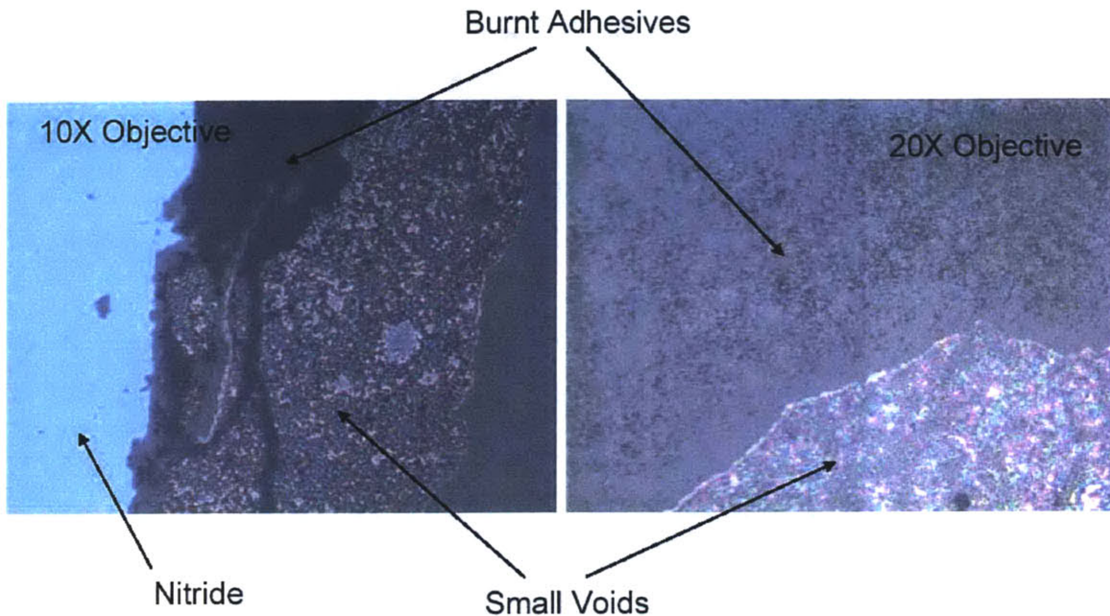

Figure 6-7. Misleading Glass Frit Bond

With optimized pre-sintering and bonding parameters, several attempts were made at packaging devices but no vacuum was achieved. Recalibrating one of these devices showed that the package was moderately successful in producing a hermetic seal. After sitting in a vacuum of 10mTorr for 3 days, the pressure within the package remained above 1Torr but a small leak was detected. This result led to the belief that outgassing of the frit and the interior surface of the package was responsible for the high pressures measured. Another experiment was carried out to determine if the inclusion of getters would improve the package but it was determined that the amount of getters that can fit into the getter cavity was insufficient to pump down the package.

A subsequent experiment was performed where a device was bonded twice; once for the top cap, and another time for the bottom cap with getters. This was in hopes that the two step process would eliminate half the outgassing, and possible prevent saturation of the getters. Surprisingly, this method was able to achieve a vacuum of <150mTorr but the vacuum quickly degraded. Figure 6-8 shows the recalibration data plotted against the original calibration. The sloping of the post-bond curve is representative of a small leak in the package. An SEM of the bond exposed small voids that are on the order of 10um, explaining the slow leakage detected. It might be possible to eliminate the formation of these micro-voids through extremely fine control of the bonding process but there is still the issue of outgassing that needs to be addressed.

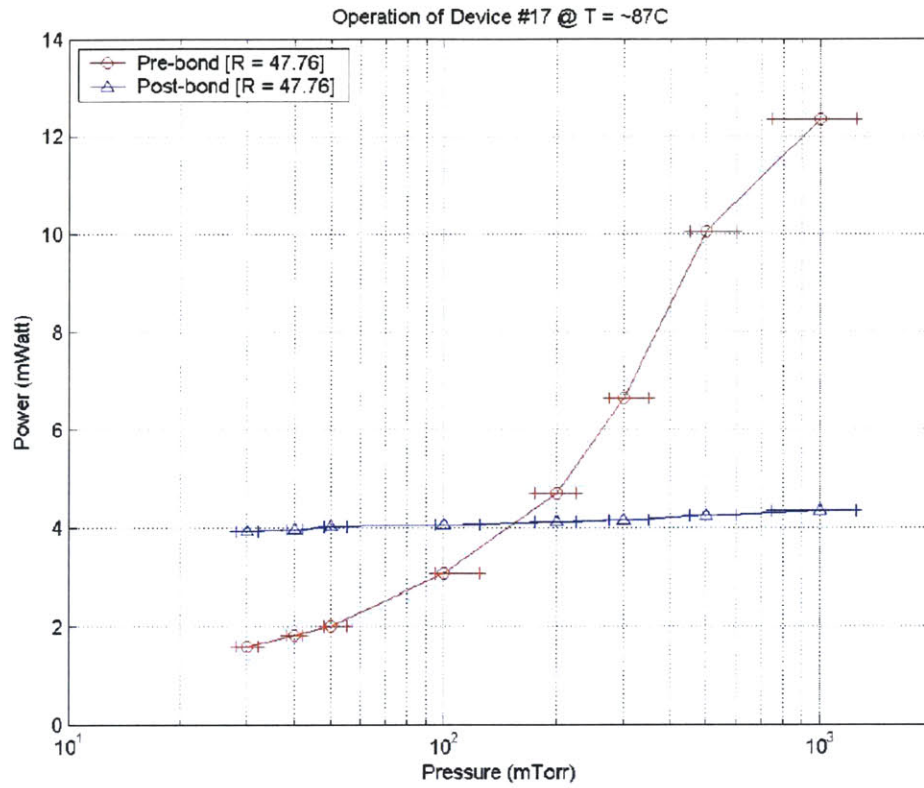

Figure 6-8. Experimental Result Showing Leaky Vacuum Package

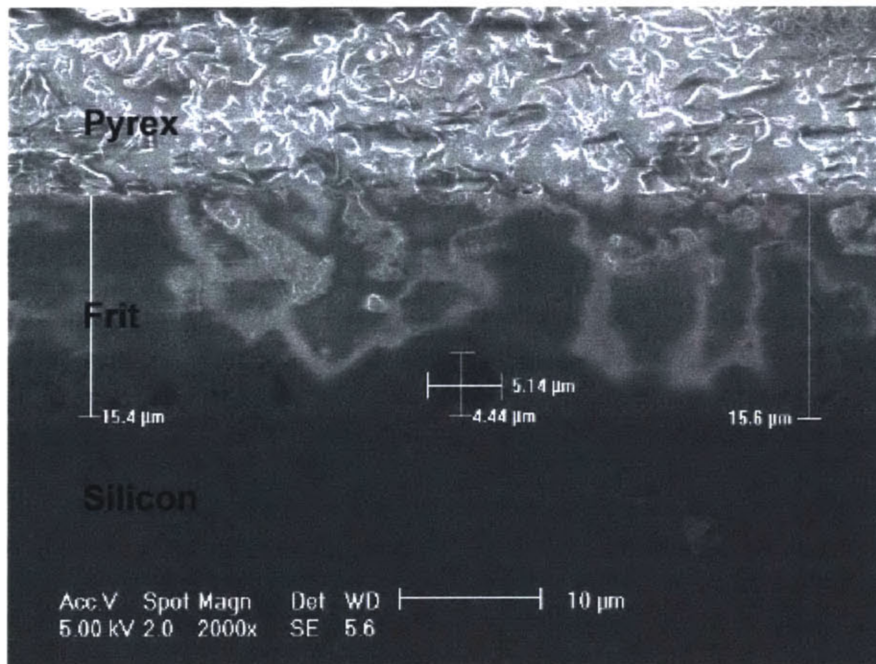

Figure 6-9. SEM of Optimized Bond

6.4 – Two-Step Bonding

6.4.1 – Setup

The initial bonding is performed in a box furnace (Thermolyne 48000) that has a built in temperature controller that can be programmed to achieve a multi-stepped heating process. A stainless steel bonding chuck is made with a similar design to the copper chuck in Figure 6-6. Copper was not used since it will oxidize, flake, and potentially obstruct the bonding. Aluminum shadow mask are made for the deposition of the wetting layers in the solder experiments. These components are shown in Figure 6-10 and the dimensions are provided in Appendix E.

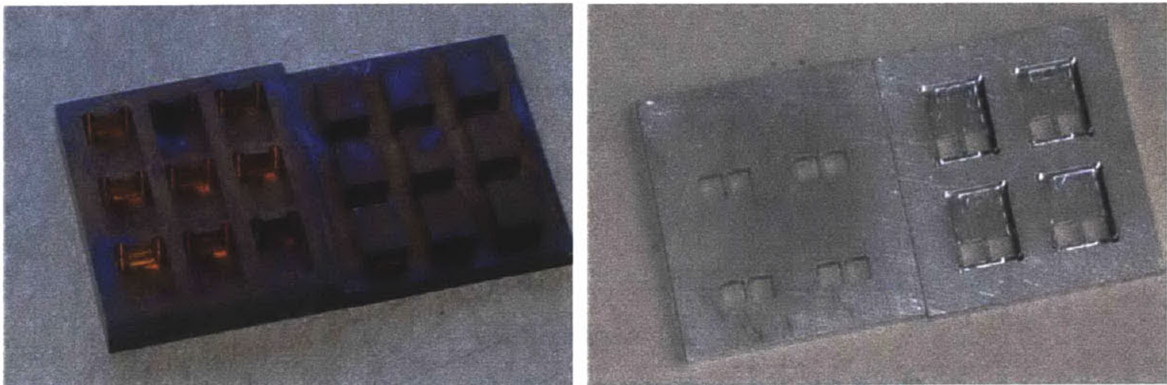

Figure 6-10. Machined Bonding Chuck and Shadow Mask

Bonding in the box furnace was optimized with a similar methodology prescribed in Chapter 3. The results and images from this work are compiled in Appendix F. It was ascertained that a peak temperature of 525°C and a hold time of 30 minutes will produce a bond that is similar to the optimized bond of Chapter 3. A problem encountered when 7kg of weights were used to bond four devices at a time was that the caps failed to bond. It was determined that the weights served as large thermal masses that pulled heat away from the bonding chuck, thus preventing the samples from reaching the ideal bonding temperature. To solve this problem, the heating cycle was changed to the process outlined in Figure 6-11, and the bonding configuration shown in Figure 6-12 was used to manage heat distribution. Slight unevenness in the applied pressure was noticed but incorporating spacers made from Grafoil, flexible graphite developed by GrafTech International, will be able to correct this if the unevenness becomes a significant issue.

The final seal-off utilizes a similar setup as the vacuum bonding. The bonding chucks are inverted to provide two flat surfaces that will serve as hot plates. The packaged device is loaded with the seal-off material and pinched in-between the chucks as shown in Figure 6-13. The device is placed so the pump-out holes are exposed, allowing for the visual inspection of the seal-off process. Small weights are used to ensure good thermal contact between the chuck and device, while the ceramics are used for thermal isolation. The system is pumped down and the bonding chucks are heated until the seal-off material melts.

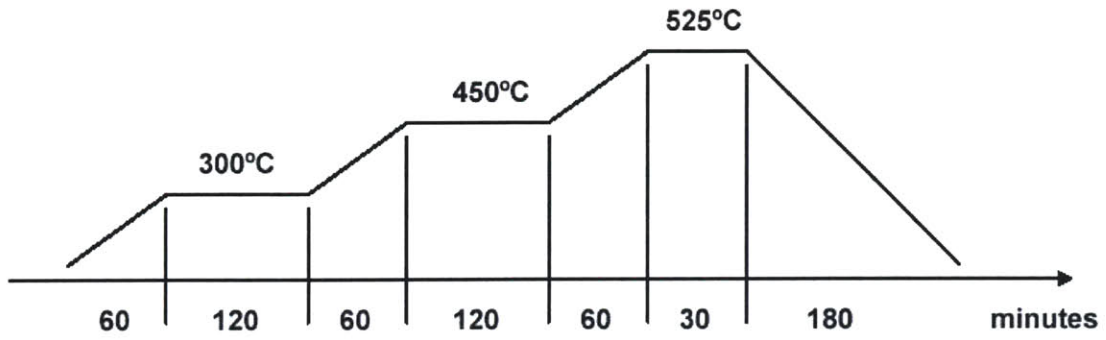

Figure 6-11. Modified Heating Cycle

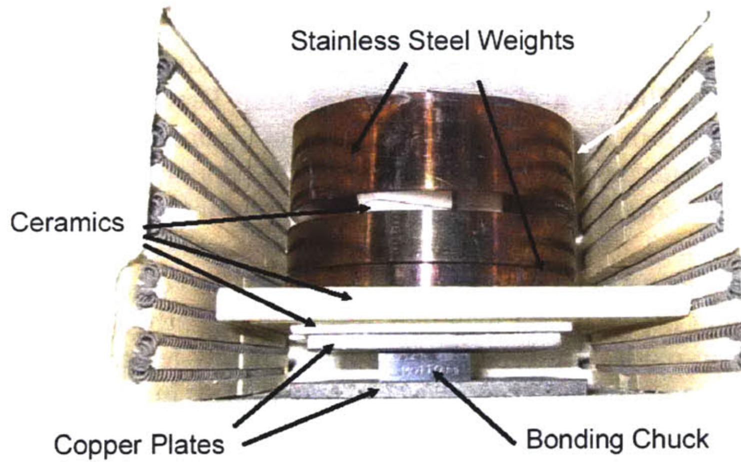

Figure 6-12. Box Furnace Bond Setup

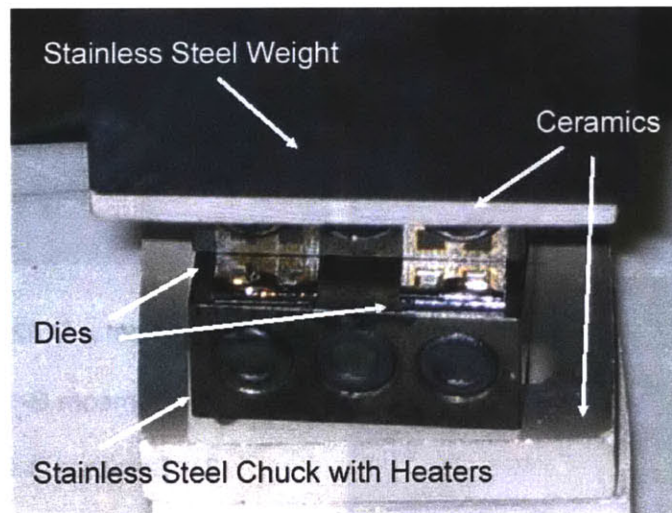

Figure 6-13. Final Seal-Off Setup

6.4.2 – Results

After the box bond process had been optimized, several devices were packaged using capping dies from the vacuum bond process. The purpose of these experiments was to evaluate if the box bonding technique could achieve hermeticity. If devices are packaged at atmosphere and subsequently recalibrated in vacuum, a leak will manifest itself as a change in the power dissipation of the sensor. All the packaged devices demonstrated hermeticity over the evaluation time of 24+ hours. This conclusion was arrived at since the devices exhibited a constant value for power dissipation regardless of pressure and time. The next set of experiments involved heating these devices using the final seal-off setup. These experiments were conducted to determine if the seal-off process would degrade the hermeticity achieved in the initial bond. All the devices retained hermeticity after being heated at 450°C for 30+ hours. With these promising results, attention was turned to evaluating the final-seal off materials.

The first set of materials evaluated were the low melting glass frits. The results of the seal-off with DM2700PF, a glass frit preform from Diemat Inc., B-10105, and B-10127, glass powders from Semcom Inc., are shown in Figure 6-14. DM2760PF was not evaluated since the material was unavailable from the vendor. Ideal behavior for these glasses would be well controlled reflows at the melting point but "boiling" was observed for all these materials. This "boiling" introduces many bubbles in the seal-off material, forming leakage pathways into the package. It was observed that once the "boiling" subsided, the melting points of the materials were significantly higher than the original values. Since boron-oxide is a typical component of low-temperature glasses, it was concluded that this component decomposes when heated in a vacuum environment, producing the "boiling" phenomenon observed. This material decomposition can also explain the micro-voids displayed in Figure 6-9 as well as the significant issue with void formations in the work of Chapter 3.

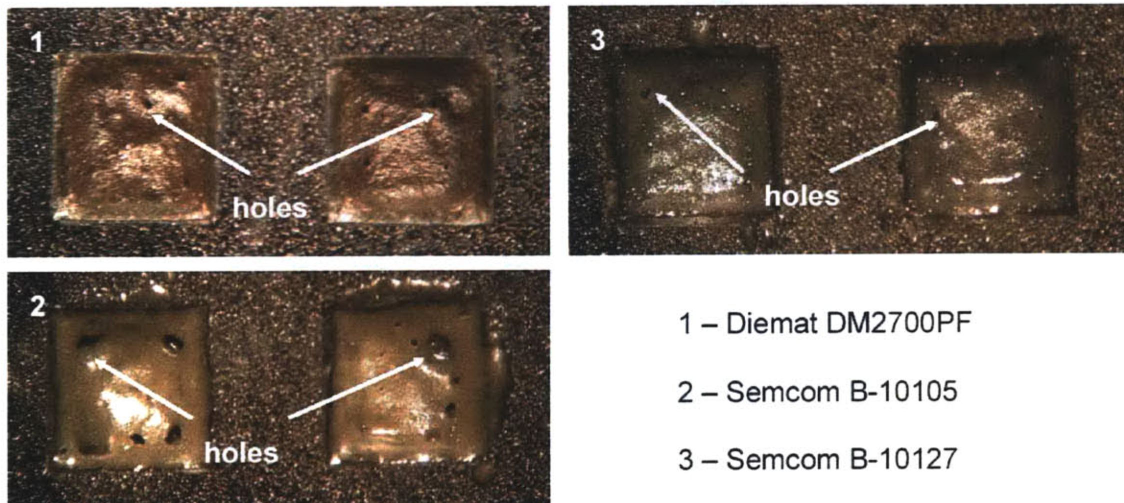

Figure 6-14. Final Seal-Off with Low Melting Glass

With the unsuccessful attempts with the low melting glasses, attention was turned to the use of solder. Due to material costs issues, only a small sample of gold-indium (82/18) was obtained. The sample came as a thin sheet that was subsequently cut into small rectangular pieces with a scissor. This step was necessary so that the solder material could fit into the pump-out holes. A sample wire of gold-tin (80/20), a gold-based solder with a eutectic temperature of 280°C, was provided by a fellow lab member. Since this material is a close fit to the constraints outlined in Chapter 4, it was also investigated.

A simple layer of 10nm Ti/100nm Au was initially used as the wetting metal but the solder failed to wet the walls of the pump-out holes. This result is likely due to the formation of a gold-silicon eutectic from the diffusion of silicon into the gold. A new wetting layer consisting of 30nm Ti/500nm Ni/300nm Au was utilized, producing the results shown in Figure 6-15.

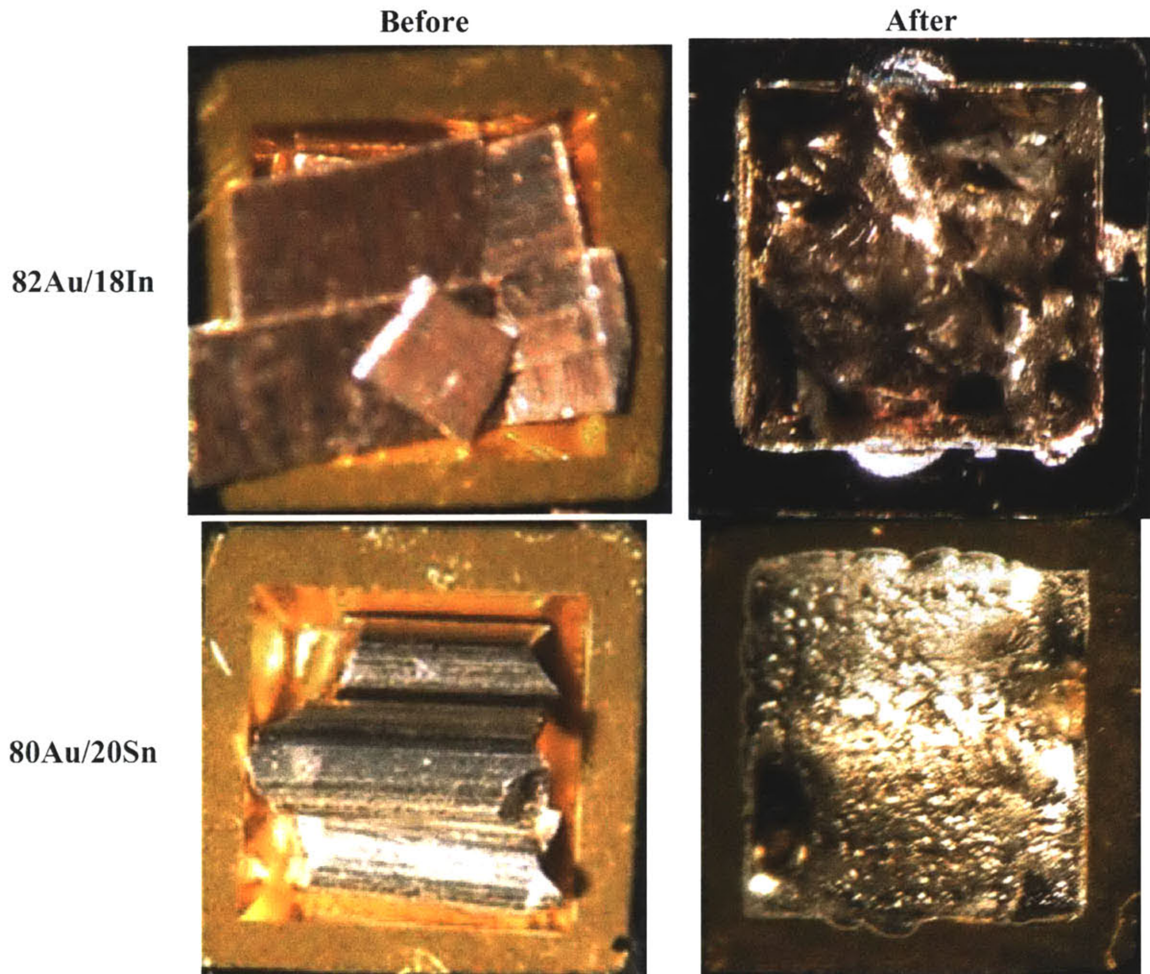

Figure 6-15. Final Seal with Solder

The solders were placed into the pump-out holes and the heating chuck is rapidly ramped to the working temperature of the material, namely 485°C for the gold-indium and 280°C for the gold-tin. Once the solder is observed to melt and reflow, the power is turned off and the pieces were allowed to cool in the vacuum chamber. It was noticed that the gold-indium fails during the seal-off process since it does not melt completely. Speculation for this result is that the increased surface area of the "glitter" allows for the rapid diffusion of the gold wetting layer into the solder. The change in local composition can result in various melting points, with a higher gold concentration raising the melting temperature, producing the image shown in Figure 6-15. A more ideal solder preform, such as a sphere, can potential resolve this issue.

Gold-tin appeared to work significantly better than the gold-indium. This can be due to the formation of a eutectic at the working temperature, facilitating the reflow process. In all the samples sealed, holes would form around the edges of the pump-out holes and a proper seal-off could not be achieved. Speculation for the formation of these leakage pathways is the outgassing of the interior surface of the cavity during the quick ramp up. Attempts at outgassing the interior prior to seal-off were ineffective as can be seen in Figure 6-16. It appears that 500nm of Nickel is not sufficient to prevent silicon diffusion into gold when heated at 200°C for two hours. A gold-silicon eutectic must have formed which prevented the solder from wetting. A barrier layer under the wetting metal that can prevent silicon diffusion should be sufficient to resolve the formation of holes in the seal-off solder.

Figure 6-16. Gold-Tin Seal-Off with Extended Outgassing

Chapter 7
Future Work

The work conducted so far has not been able to produce a vacuum package but we are very far from exhausting all possible options. The promising results reported with solder need further exploration. The incorporation of a barrier layer under the wetting metal can potentially be used to prevent the gold-silicon eutectic formation during an extended outgas step. Work by Tsau stated that a thermal oxide layer of 150nm is sufficient to prevent silicon diffusion into gold [6]. In addition to making a new bottom cap with the oxide layer, it is possible to explore the deposition of other material that can potentially serve as a good barrier material.

Another issue with the solder experiments is not having an appropriately shaped solder preform. The crude method of solder placement in the pump out holes can be a source for potential issues. An adequately sized sphere or cube of solder that fits nicely into the pump-out holes could possibly improve the reflow and seal process. Other than the shape of the solder, there are many other metal choices to explore. Sealing off with gold-indium has not been studied thoroughly, and solders that are not gold-based could potentially be used. It might also be possible to find a low melting glass that does not contain boron-oxide, or perhaps other materials that would adequately seal the holes.

Due to the new packaging scheme, it is possible to bond an additional piece of silicon or glass directly over the bottom cap to perform the seal-off as shown in Figure 7-1. Bonding methods such as gold thermocompression bonding, eutectic bonding, and anodic bonding can now be used when deemed incompatible for the scheme developed by Chou [8]. An advantage of using these techniques is that they are well studied and do not outgas. Gold thermocompression bonding and eutectic bonding can be implemented in the current vacuum bonding apparatus. Anodic bonding would require the placement of an anodic bonder in a vacuum environment which is feasible.

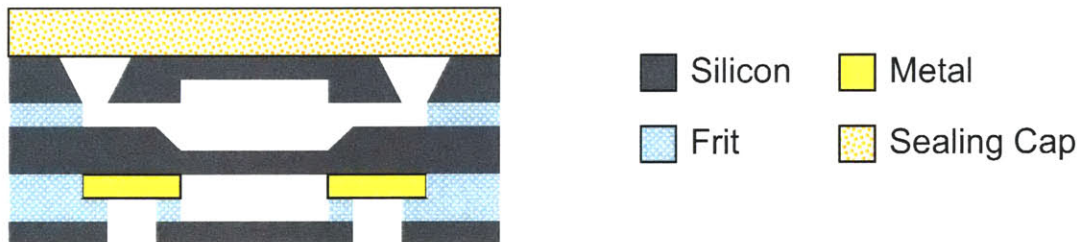

Figure 7-1. Potential Seal-Off Scheme

Choosing a glass frit other than GPR-10 for bonding is an option that is still available. Switching glass frit requires additional work for bond optimization but can prove to be quite beneficial. Utilizing a material with a higher working temperature will

open the door to other seal-off options. In addition to a larger temperature constraint for solder/frit selection, work done by Brandon Blackwell at MIT on glass tube brazing can be incorporated. Figure 7-2 shows tubes that are brazed to the fluidic ports of a micro-reactor. This technique can be used to hermetically braze tubes over the pump-out holes of the new packaging scheme. The interior cavity can be pumped out through the tubes and a tip-off can be used to seal the structure.

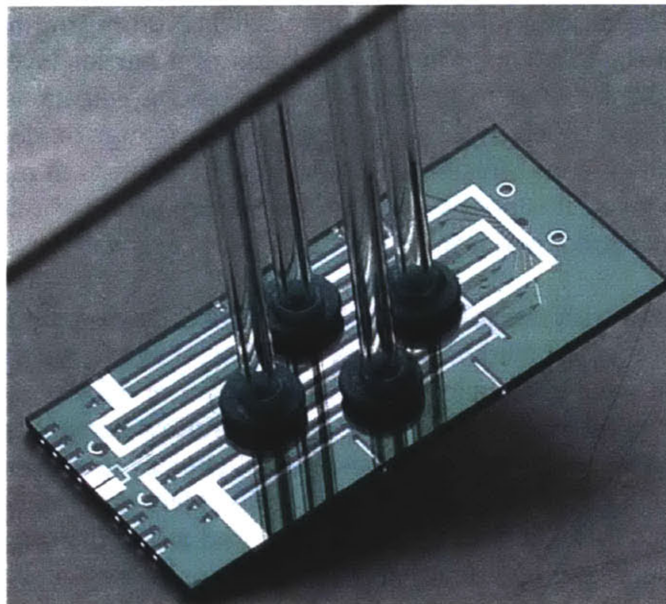

Figure 7-2. Glass Tube Brazing

Other than the work mentioned above, a more effective and efficient system to optimize the pre-sintering and bonding parameters can be planned out. The effect of surface treatments on the glass frit bond quality is another direction that can be investigated. Once a reliable packaging scheme is achieved, improvements through the incorporation of getters can be explored.

Chapter 8
Conclusions

The investigation of glass frit vacuum packaging for the thermal management of a micro-fuel processor has been continued. Unfortunately, a reliable vacuum package has not been achieved to date. Several issues with the prior work has been addressed and resolved, and a new packaging scheme is developed and explored.

Significant work was performed to improve the bond quality of the packaging scheme developed in the previous work. A study of the effects that bonding conditions had on void formation was conducted. An optimization methodology was developed and used to decrease the size of the voids formed in the frit layer during bonding. Pre-sintering and bonding parameters were successful optimized for GPR-10 and used to produce a voidless glass frit bond. The optimized seal produced a vacuum package with an initial pressure of <150mTorr but with unreliable hermeticity.

A new and versatile packaging scheme using a two-step process is proposed and investigated to address the issues of outgassing. Glass frit bonding in a box furnace has been demonstrated to produce a reliable, hermetic seal. Packaged devices retained hermeticity even after being heated at 450°C for over 30 hours. The use of glass preforms, glass frits, and solders were explored for the final seal-off step. The low melting glasses failed to seal properly but the use of solder appear to be quite promising. A vacuum package with the new packaging scheme has yet to be achieved but there is confidence that a solution will be found with additional work.

Appendix A
Modeling of Sensor

The underlying principle used to develop this model is the conservation of energy. Power dissipated in the resistor must equal the heat flux away from the resistor. Heat conduction along the nitride membrane, radiation from the heater, and conduction through gases are the primary heat transport mechanisms. For simplicity, convection in gases is assumed negligible. This model takes into account classical and size effects since some of the relevant dimensions are small.

Theory

Conduction along Membrane

Heat conduction along the membrane is treated using Fourier's Law. Assuming the nitride is an isotropic material and the boundaries are diffusely scattering, we can obtain an equation relating thermal conductivity and dimensions. For a free standing thin film, the phonon thermal conductivity with diffusely scattering boundaries is given by [15],

$$\frac{k}{k_b} = 1 - \frac{3}{8\xi}\left[1 - 4\left\langle E_3(\xi) - E_5(\xi)\right\rangle\right] \quad ; \quad E_n(x) = \int_0^1 \mu^{n-2} \exp\left(-\frac{x}{\mu}\right) d\mu \qquad (1)$$

where k_b is the bulk thermal conductivity of the material, $\xi = d/\Lambda$ is the acoustic thickness, d is the thickness of the film, and Λ is the phonon mean free path in silicon nitride. To estimate the value of the phonon mean free path, the simple kinetic theory can be used to obtain $k_b = Cv\Lambda/3$, where C is the volumetric specific heat and v is the speed of the carrier in the material [15]. Another option is to utilize the equipartition theorem to derive,

$$\Lambda = \frac{2hv}{\kappa_B T} \qquad (2)$$

where h is Planck's constant, κ_B is Boltzmann's constant, and T is the temperature of the material [16].

Transport by Radiation

Heat flux from radiation can be modeled rather simply by assuming parallel plate geometry and utilizing the Stefan-Boltzmann Law for radiation. Assuming the diffusion approximation is applicable and diffusion-transmission boundary conditions are used, the need to solve for the temperature distribution within the medium is avoided. The heat flux, J_q, between two parallel surfaces is then given by [15],

$$\frac{J_q}{e_{01}-e_{02}}=\frac{1}{\frac{3dK_e}{4}+\frac{1}{\varepsilon_1}+\frac{1}{\varepsilon_2}-1} \quad ; \quad K_e=\frac{4\pi\kappa}{\lambda_0} \tag{3}$$

where $e_{0n} = \sigma T^4_n$ is the black body radiation of the nth surface at temperature T_n (σ being the Stefan constant), ε_n is the emissivity of the nth surface, d is the spacing between the surfaces, and K_e is the extinction coefficient of the radiation. In Equation 3, κ is the material extinction coefficient, and λ_0 is the photon wavelength which can be estimated using Equation 2 (for photons, the 2 in the numerator is replaced by 0.15), or the Wein's Displacement Law $\lambda_0 T = 2167.8\mu m \cdot K$ [15].

Conduction through Gases

Conduction through the gases held in the package can also be modeled using the simple Fourier's Law. We have a rarefied gas trapped between parallel plates due to the large mean free paths at low pressures. Utilizing the diffusion approximation and diffusion-transmission boundary conditions, the thermal conductivity is given as [15]

$$\frac{k}{k_b}=\frac{1}{1+\frac{4\Lambda}{3d}} \tag{4}$$

In the situation of a gas, the mean free path is dependent on pressure. From the kinetic theory of gases, we have

$$\Lambda=\frac{\kappa_B T}{\sqrt{2}\delta^2 P} \tag{5}$$

where δ^2 is the collision cross-sectional area of the gas molecules, and P is the pressure of the gas [8].

Combining all three heat transport mechanisms and equating it to the power dissipated in the resistor, we have

$$Power = I \cdot V = \frac{A_{cs-nit}k_{nit}(T-T_0)}{L_{nit}}+\frac{A_{c-top}k_{air}(T-T_0)}{d_{top}}+\frac{A_{c-bot}k_{air}(T-T_0)}{d_{bot}}+ \\ A_{r-top}J_{r-top}+A_{r-bot}J_{r-bot} \tag{6}$$

I is the current being passed through the device, V is the voltage measured across the device, T is the effective peak temperature of the device and T_0 is the temperature of the package. A_{cs-nit} is the effective cross section area that heat is transported across the membrane, k_{nit} is the thermal conductivity of the membrane, and L_{nit} is the effective distance along the membrane that the temperature gradient is established. $A_{c-top/bot}$ is the

effective cross sectional area of the air conduction pathway above/below the resistor, k_{air} is the pressure dependent thermal conductivity for air, and $d_{top/bot}$ is the distance from the resistor to the top/bottom of the package. $A_{r\text{-}top/bot}$ is the effective surface area that is emitting radiation above/below the resistor, and $J_{r\text{-}top/bot}$ is the corresponding heat flux above/below the membrane.

Results

From an extensive literature search, several values for material properties were extracted and are summarized in Table A-1 along with assumed dimensions used in the model. Most material properties depend on temperature so the values chosen correspond to those at $T = T_{avg} = 330°K$, the average between the temperature of the package (room temperature) and the target temperature of the sensor in a constant temperature operation mode (360°K ~ 87°C).

Table A-1. Material Properties and Dimensions [16-18]

$k_{nit\ 0}$	3.0 W/K-m		L_{nit}	100×10^{-6} m
$C_{v\text{-}nit}$	1.14×10^{6} J/m^3-K		d_{nit}	100×10^{-9} m
$v_{nit\text{-}l}$	10.3×10^{3} m/s		d_{top}	25×10^{-6} m
$v_{nit\text{-}t}$	6.2×10^{3} m/s		d_{bot}	450×10^{-6} m
$k_{air\ 0}$	0.0285 W/K-m		$A_{r/c\text{-}top/bot}$	$(1.2 \times 1.2) \times 10^{-6}$ m^2
δ^2	4.39×10^{-19} m^2		$A_{cs\text{-}nit}$	$4(1.2 \times 100) \times 10^{-12}$ m^2
$\varepsilon_{nitride}$	0.18		$\varepsilon_{platinum}$	0.05
$\varepsilon_{silicon}$	0.65			

Utilizing the simple kinetic theory, the mean free path for phonons in the nitride film was calculated to be Λ_{nit} = 1.27nm assuming that the translational mode is the dominant mode for phonons. If Equation 2 was used instead, we would obtain Λ_{nit} = 1.80nm which is on the same order of the value obtained from the kinetic theory. In either case, the acoustic thickness ξ is relatively large indicating that the thermal conductivity of the film is close to that of bulk nitride. Assuming that the heat transport along the membrane is isotropically away from the resistor, the heat conduction along the nitride film is calculated to be 0.864mW.

Since air is the medium in which radiation is passing through, the material extinction coefficient κ is zero, simplifying the expression in Equation 3. The photon wavelength is not needed but we can calculate the estimated values for completeness. We obtain 6.55um using the photon version of Equation 2 (replace the 2 with 0.15) while we get 6.57um using the Wein's Displacement Law. These two values are very close and are on the order of d_{top}, indicating that classical effects can potentially be important if the gas did not have a zero extinction coefficient. Assuming that the nitride directly beneath the platinum reaches the same temperature as the resistor, the total radiation is calculated to be 0.151mW.

From Figure A-1, we can see that conduction through gases is the dominant heat transport mechanism in the packaged device. A quick calculation shows that the mean free path of air is 55um at P = 1,000mTorr, and is 5.5mm at P = 10mTorr. Since the mean free paths at the pressures of interest are larger that d_{top}, there is no doubt that the rarefied gas treatment is necessary.

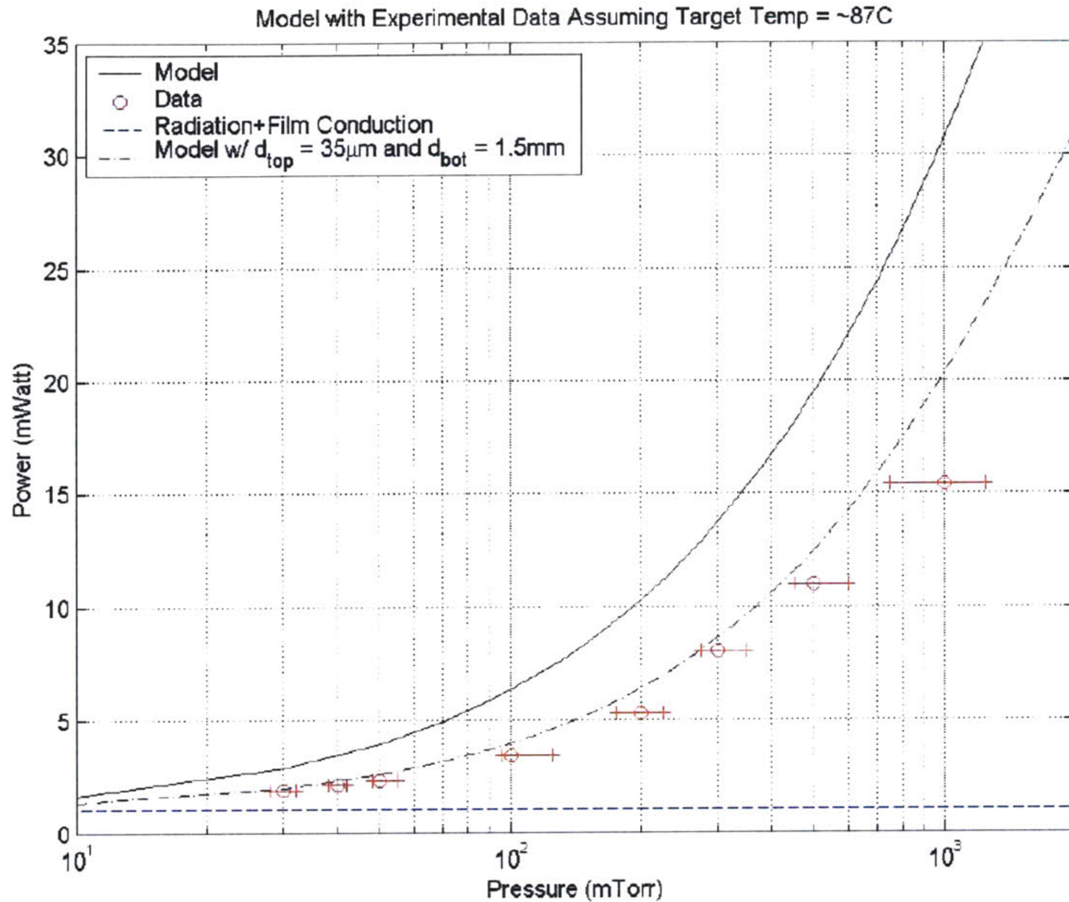

Figure A-1. Model with Experimental Data

Discussion

Looking at the experimental data in Figure A-1, we see that at low pressures, the power dissipated in the test structure approaches the dashed line. This line corresponds to the heat conduction across the membrane and of radiation. Since the heat conduction through gases should approach zero as the package pressure approaches a pure vacuum, we would expect the data to be limited by the value indicated by the dashed line. Such a result would indicate that the modeling of the two heat transport mechanisms represented by the dash line is quite accurate, but we must keep in mind the inaccuracies introduced by the assumptions made.

Several crude assumptions were made in developing this model. The values for the effective cross sectional areas used in the calculation, and the assumption of a constant temperature distribution across the resistor are gross oversimplifications. Assuming that the heat in the resistor is completely transferred to the nitride membrane may be inaccurate since there will be some finite heat conduction along the metal lines. It is also assumed that the bulk silicon package remains at room temperature, and that there are no thermal boundary resistances in the system. Introducing thermal boundary resistances will present finite temperature differences at the various interfaces, invalidating the assumptions made about the temperature distribution as well as the importance of convection. Utilizing perfectly diffusive boundaries and perfectly planar surfaces makes modeling the system easier but introduces many inaccuracies.

Despite the assumptions, the pressure dependence of the heat conduction through gases correlates fairly well to the experimental data. We see that the discrepancies are smaller at lower pressures and greater at higher pressures. A possible explanation is the lack of instrumental precision at the higher pressures. Another explanation is that the assumptions used to arrive at Equation 4 were poor. The thermal conductivity of air is strongly dependent on the value used for d_{top} and d_{bot}. Since the packaged device does not comprise of infinite parallel plates, the effective distances can be greater than those used in the calculation. As seen in Figure A-1, increasing the values for d_{top} and d_{bot} can potentially increase the correlation between model and experimental data by a significant amount.

Appendix B
Non-Evaporable Getter (St122)

Non-Evaporable Getters (NEG) are very useful since they can be exposed to air prior to usage. The getter intended for use is St122-NCF-A4-I500-800/50-75/1x1/S which is manufactured by SAES Getters Inc.. As can be seen from Figure B-1, this product is a high porosity thin film of Ti with Zr-V-Fe that sits on a $1mm^2$ nicrofer substrate. The increased surface area from the high porosity combined with the chemical reactivity of the thin film components produces a material that features high sorption capacity to active gases such as H_2, O_2, N_2, CO, and H_2O vapor. Performance data for this product is shown in Figure B-2.

The recommended use of this product with MEMS packaging is a bake-out of the caps followed by the activation of the getters in a vacuum environment prior to sealing. Baking the caps will drive out residual gases that can outgas into the package, decreasing the lifetime of the getters. The activation step is a thermal process that is used to diffuse the passivation layer on each grain into the bulk material. This diffusion process is a function of time and temperature, and can affect getter performance as summarized in Figure B-3.

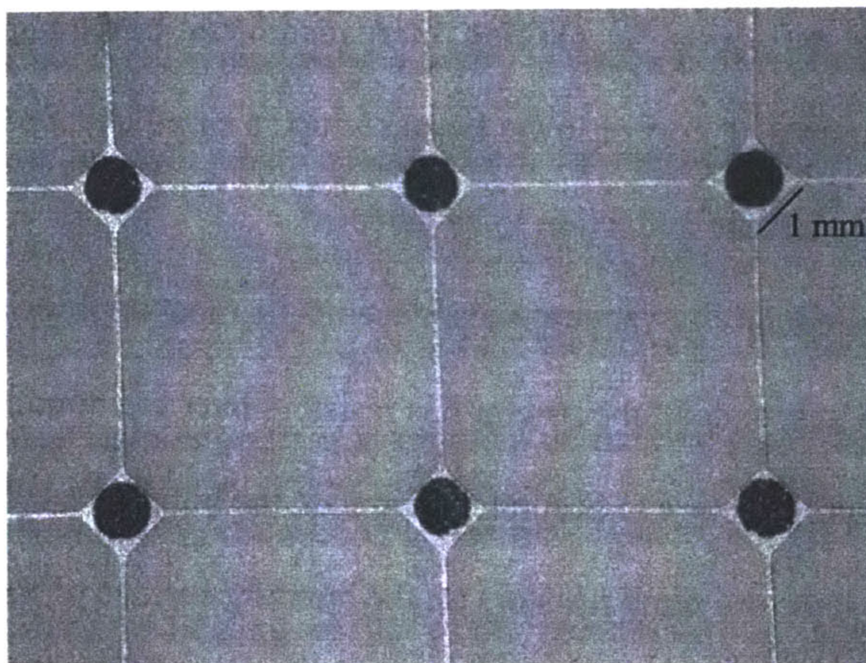

Figure B-1. St122 Non-Evaporable Getters

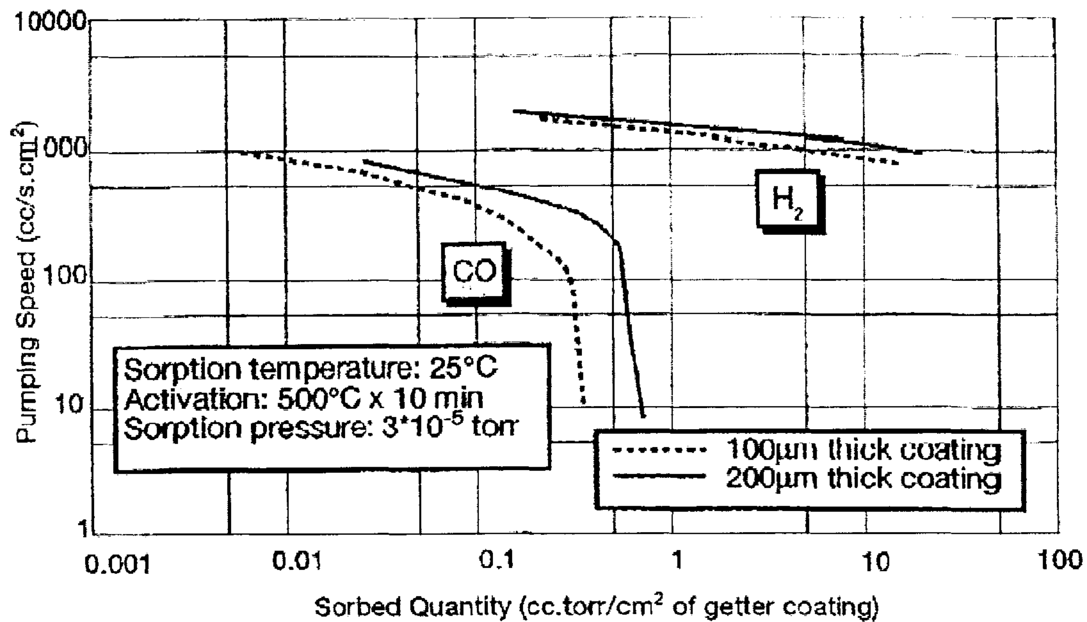

Figure B-2. Getter Performance

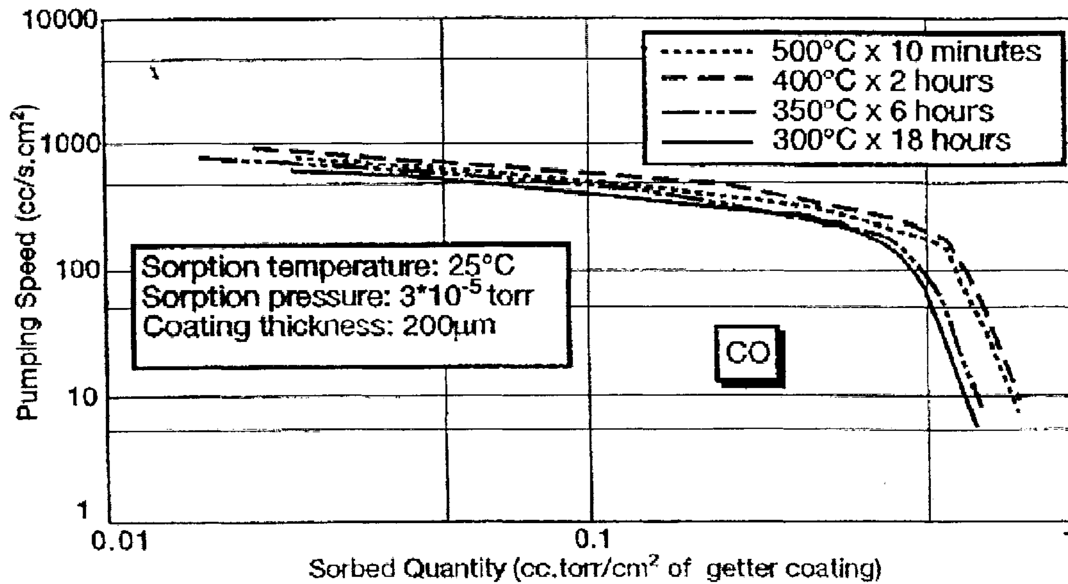

Figure B-3. Getter Activation

Appendix C
Process Flows

TOP CAP (4" SSP)				
RCA Clean		RCA	ICL	
Grow SiO2 (0.5um)		TUBE 5C	ICL	
Polished Side Processing				
HMDS		HMDS	TRL	
Coat PR (OCG825, pos, 1um)		COATER	TRL	
Prebake PR (30min @ 90C)		PREBAKE OVEN	TRL	
Expose (Cavity @ 1.8s)		EV1	TRL	
Develop PR		PHOTOWET-L	TRL	
Paint backside with OCG825		PHOTOWET-L	TRL	
Postbake PR (30min @ 120C)		PREBAKE OVEN	TRL	
Remove SiO2 (BOE)		ACID HOOD	TRL	
Mount to Handle Wafer (6" Quartz, Target)		COATER	TRL	
Bake (20min @ 90C)		PREBAKE OVEN	TRL	
Etch Cavity (~15um)		STS2	TRL	
Dismount Handle Wafer (Acetone Soak)		ACID HOOD	TRL	
Remove PR (Piranha)		ACID HOOD	TRL	
Unpolished Side Processing				
HMDS		HMDS	TRL	
Coat PR (OCG825, pos, 1um)		COATER	TRL	
Prebake PR (30min @ 90C)		PREBAKE OVEN	TRL	
Expose (Contact Holes @ 1.8s), back-side align		EV1	TRL	
Develop PR		PHOTOWET-L	TRL	
Paint backside with OCG825		PHOTOWET-L	TRL	
Postbake PR (30min @ 120C)		PREBAKE OVEN	TRL	
Remove SiO2 (BOE)		ACID HOOD	TRL	
Remove PR (Piranha)		ACID HOOD	TRL	
HMDS		HMDS	TRL	
Coat PR (AZP4620, pos, 10um)		COATER	TRL	
Prebake PR (60min @ 90C)		PREBAKE OVEN	TRL	
Expose (Contact Holes @ 4 x 4.8s+8.0s wait), back-side align		EV1	TRL	
Develop PR		PHOTOWET-L	TRL	
Postbake PR (30min @ 90C)		PREBAKE OVEN	TRL	
Mount to Handle Wafer (6" Quartz, Target)		COATER	TRL	
Bake (20min @ 90C)		PREBAKE OVEN	TRL	
Etch Contact Holes (Thru Wafer ~525um)		STS2	TRL	
Dismount Handle Wafer (Acetone Soak)		ACID HOOD	TRL	
Remove PR (Piranha)		ACID HOOD	TRL	

BOTTOM CAP (4" SSP)				
RCA Clean		RCA	ICL	
Grow SiO2 (0.5um)		TUBE 5C	ICL	
Polished Side Processing				
HMDS		HMDS	TRL	
Coat PR (OCG825, pos, 1um)		COATER	TRL	
Prebake PR (30min @ 90C)		PREBAKE OVEN	TRL	
Expose (Cavity @ 1.8s),		EV1	TRL	
Develop PR		PHOTOWET-L	TRL	
Paint backside with OCG825		PHOTOWET-L	TRL	
Postbake PR (30min @ 120C)		PREBAKE OVEN	TRL	
Remove SiO2 (BOE)		ACID HOOD	TRL	
Remove PR (Piranha)		ACID HOOD	TRL	
HMDS		HMDS	TRL	
Coat PR (AZP4620, pos, 10um)		COATER	TRL	
Prebake PR (60min @ 90C)		PREBAKE OVEN	TRL	
Expose (Cavity @ 4 x 4.8s+8.0s wait), front-side align		EV1	TRL	
Develop PR		PHOTOWET-L	TRL	
Postbake PR (30min @ 90C)		PREBAKE OVEN	TRL	
Mount to Handle Wafer (6" Quartz, Target)		COATER	TRL	
Bake (20min @ 90C)		PREBAKE OVEN	TRL	
Etch Getter Cavity (~250um)		STS2	TRL	
Dismount Handle Wafer (Acetone Soak)		ACID HOOD	TRL	
Remove PR (Piranha)		ACID HOOD	TRL	

DEVICE LAYER (4" DSP)				
RCA Clean		RCA	ICL	
Deposit Low Stress Nitride(100nm)		VTR	ICL	
Polished Side Processing				
HMDS		HMDS	TRL	
Coat PR (OCG825, pos, 1um)		COATER	TRL	
Prebake PR (30min @ 90C)		PREBAKE OVEN	TRL	
Expose (Membrane @ 1.8s)		EV1	TRL	
Develop PR		PHOTOWET-L	TRL	
Postbake PR (30min @ 120C)		PREBAKE OVEN	TRL	
Etch Nitride		PLASMAQUEST	TRL	*GOLD
Remove PR (Piranha)		ACID HOOD	TRL	*GOLD
Other Polished Side Processing				
HMDS		HMDS	TRL	*GOLD
Coat PR (AZ5214E, neg, 1.5um)		COATER	TRL	*GOLD
Prebake PR (30min @ 90C)		PREBAKE OVEN	TRL	*GOLD
Expose (Heaters 1.5sec)		EV1	TRL	*GOLD
Postbake PR (30min @ 90C)		POSTBAKE OVEN	TRL	*GOLD
Flood Expose (60s)		EV1	TRL	*GOLD
Develop PR		PHOTOWET-L	TRL	*GOLD
Deposit Ta(10nm)/Pt(400nm)/Ta(20nm)		E-BEAM	TRL	*GOLD
Lift-Off (Acetone Soak)		PHOTOWET-R	TRL	*GOLD

KOH (using one sided chuck @ 85C and 20%, through wafer ~525um)		KOH	SGL	*GOLD
Anneal Metal (60min @ 650C, 60min ramp-up)		BOX FURNACE	KFJL	
Spray Coat Metallization with OCG825		ACID HOOD	EML	
Bake (30min @ 90C)		POSTBAKE OVEN	EML	

TWO-STEP CAP (4" DSP)				
RCA Clean		RCA	ICL	
Deposit Low Stress Nitride(100nm)		VTR	ICL	
Polished Side Processing				
HMDS		HMDS	TRL	
Coat PR (OCG825, pos, 1um)		COATER	TRL	
Prebake PR (30min @ 90C)		PREBAKE OVEN	TRL	
Expose (Through Holes @ 1.8s)		EV1	TRL	
Develop PR		PHOTOWET-L	TRL	
Postbake PR (30min @ 120C)		PREBAKE OVEN	TRL	
Etch Nitride		PLASMAQUEST	TRL	*GOLD
Remove PR (Piranha)		ACID HOOD	TRL	*GOLD
KOH (using one sided chuck @ 85C and 20%, etch ~450um-475um)		KOH	SGL	*GOLD
Post KOH Clean (2x Piranha)		ACID HOOD	TRL	*GOLD
Nitride Strip (Hot Phosphoric Acid @ 150C)		ACID HOOD	TRL	*GOLD
Grow SiO2 (0.5um)		TUBE B1	TRL	*GOLD
Other Polished Side Processing				
HMDS		HMDS	TRL	*GOLD
Coat PR (OCG825, pos, 1um)		COATER	TRL	*GOLD
Prebake PR (30min @ 90C)		PREBAKE OVEN	TRL	*GOLD
Expose (Trenches @ 1.8s), back-side align		EV1	TRL	*GOLD
Develop PR		PHOTOWET-L	TRL	*GOLD
Paint backside with OCG825		PHOTOWET-L	TRL	
Postbake PR (30min @ 120C)		PREBAKE OVEN	TRL	*GOLD
Remove SiO2 (BOE)		ACID HOOD	TRL	*GOLD
Remove PR (Piranha)		ACID HOOD	TRL	*GOLD
HMDS		HMDS	TRL	*GOLD
Coat PR (AZP4620, pos, 10um)		COATER	TRL	*GOLD
Prebake PR (60min @ 90C)		PREBAKE OVEN	TRL	*GOLD
Expose (Trenches @ 4 x 4.8s+8.0s wait), back-side align		EV1	TRL	*GOLD
Develop PR		PHOTOWET-L	TRL	*GOLD
Postbake PR (30min @ 90C)		PREBAKE OVEN	TRL	*GOLD
Mount to Handle Wafer (6" Quartz, Target)		COATER	TRL	*GOLD
Bake (20min @ 90C)		PREBAKE OVEN	TRL	*GOLD
Etch Trenches (~250um)		STS1	TRL	*GOLD
Dismount Handle Wafer (Acetone Soak)		ACID HOOD	TRL	*GOLD
Remove PR (Piranha)		ACID HOOD	TRL	*GOLD

Appendix D
Mask Layouts

This appendix only contains images for newly designed masks. Masks used in this work that were designed in previous work have been omitted. Additional information on the old masks can be found in the thesis by Chou [8].

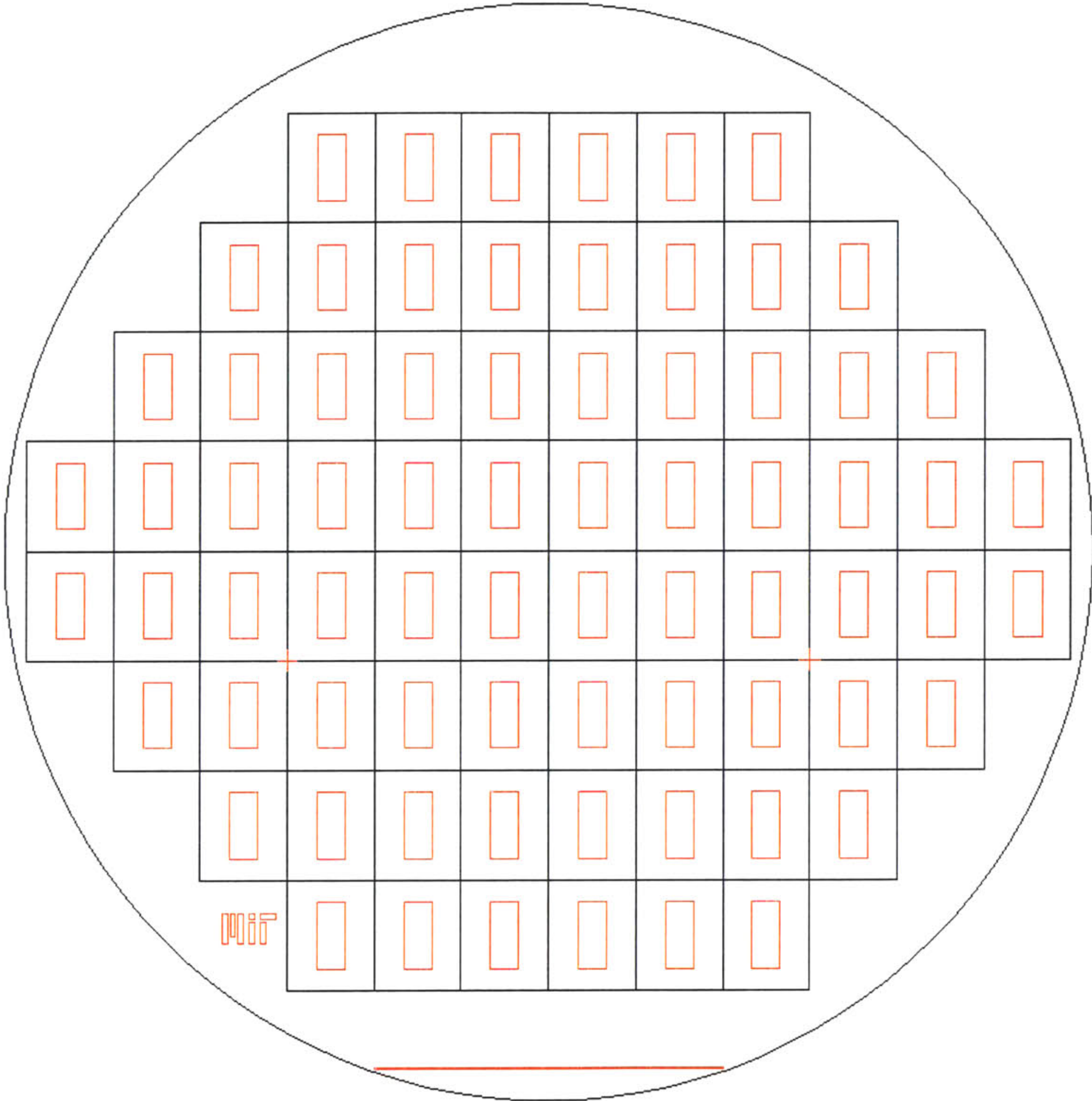

Figure D-1. Shallow Cavity of Top Cap

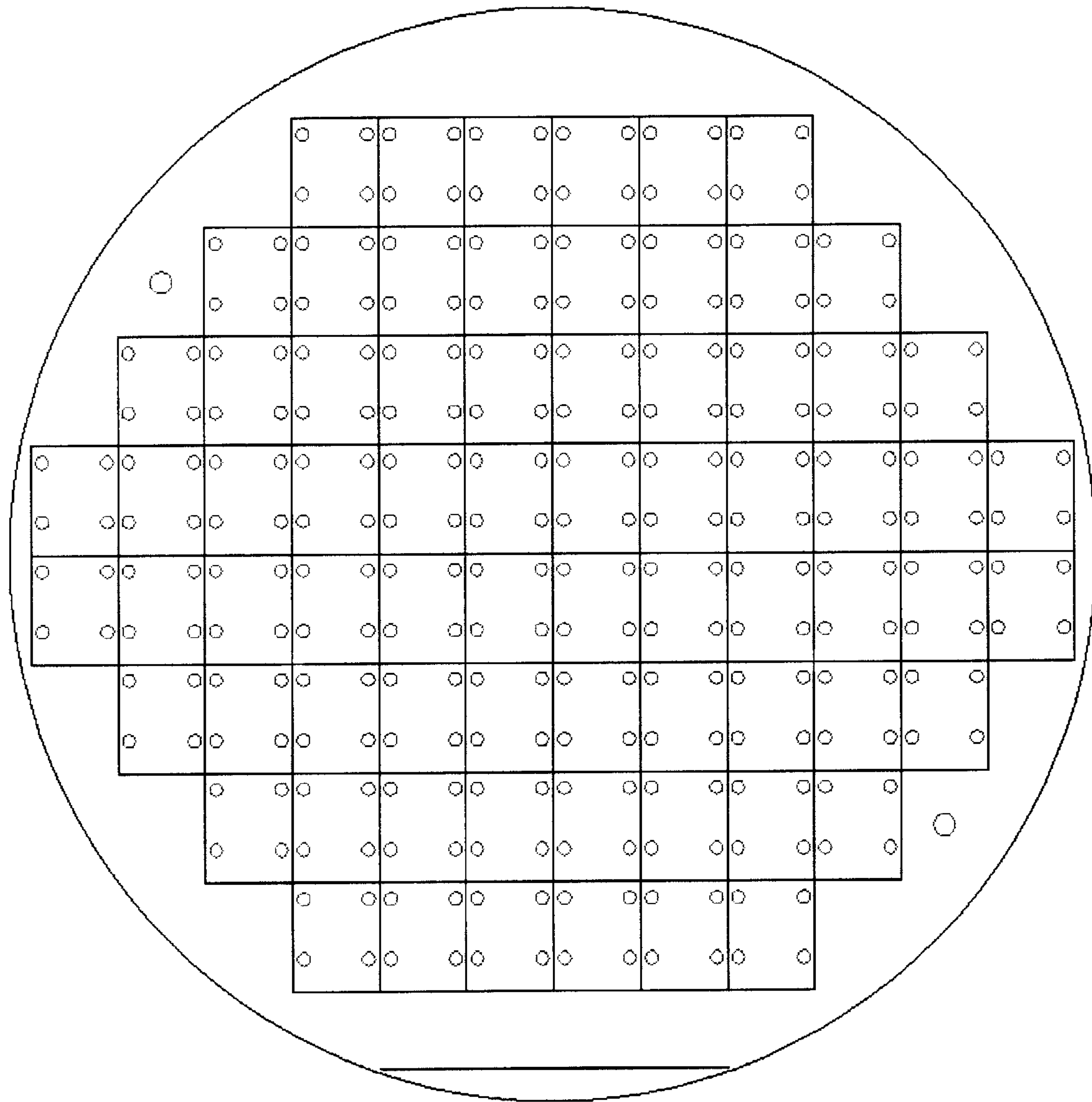

Figure D-2. Contact Holes of Top Cap

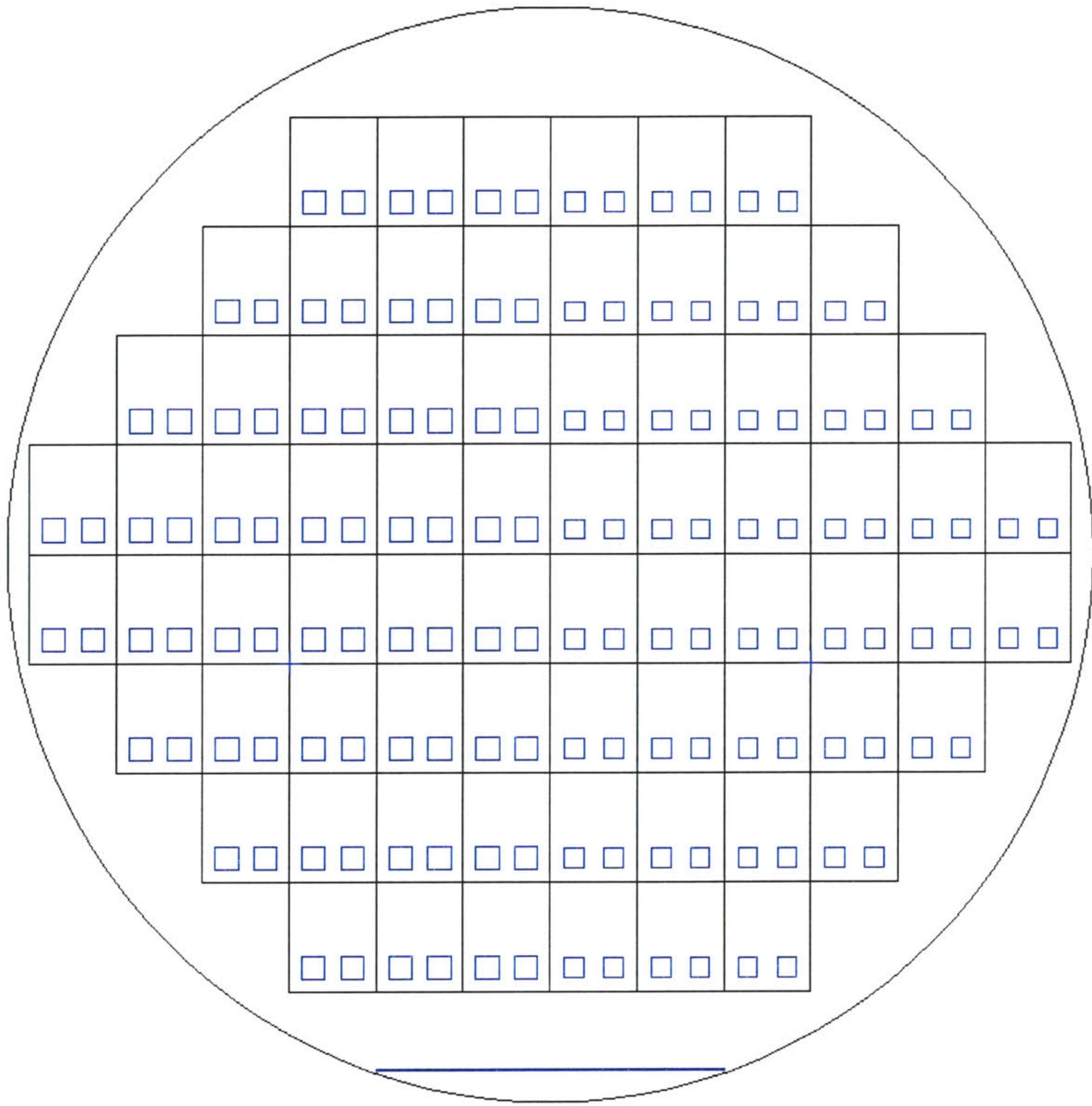

Figure D-3. Through Holes of Two-Step Cap

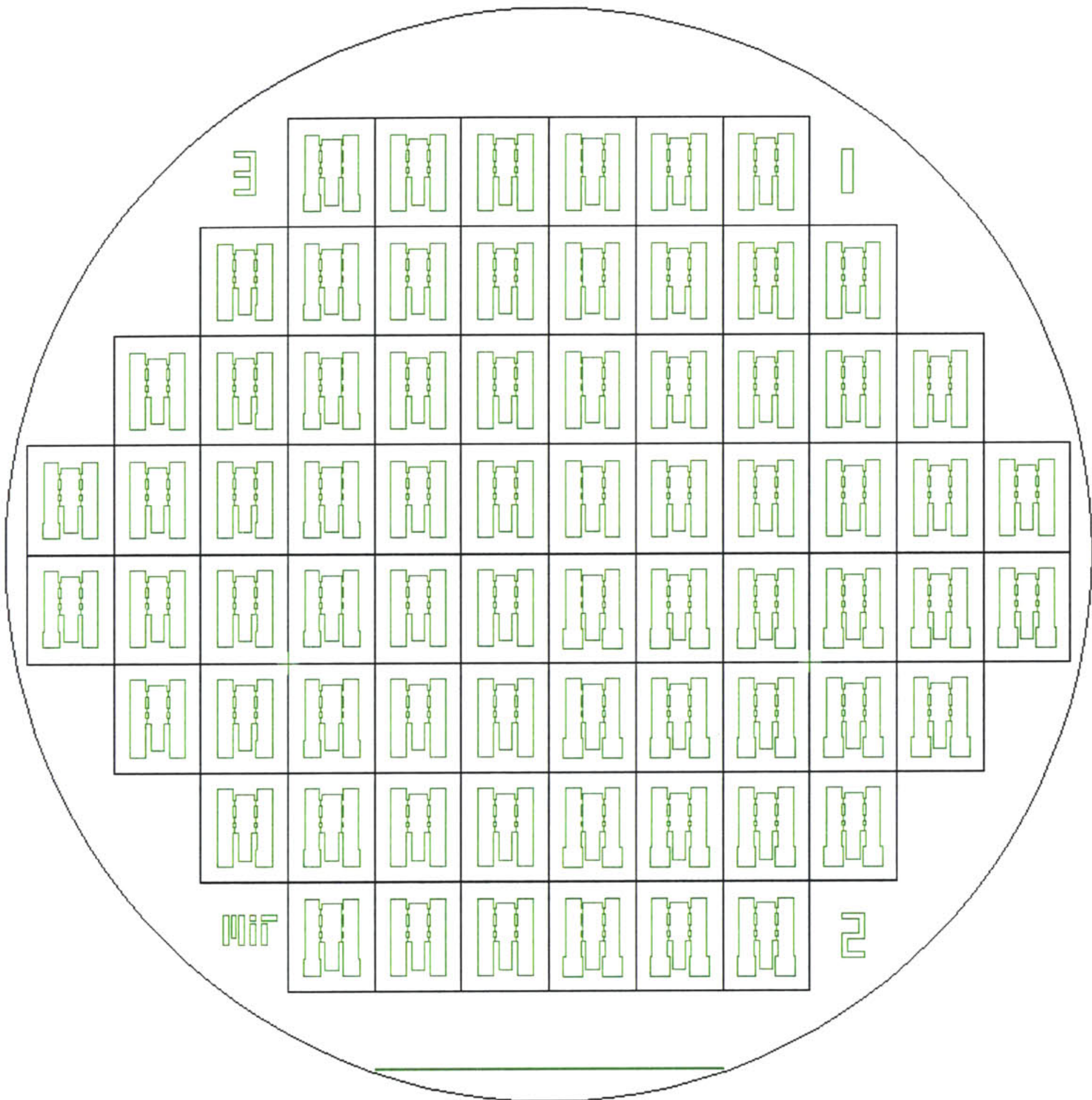

Figure D-4. Trenches of Two-Step Cap

Appendix E
Technical Drawings

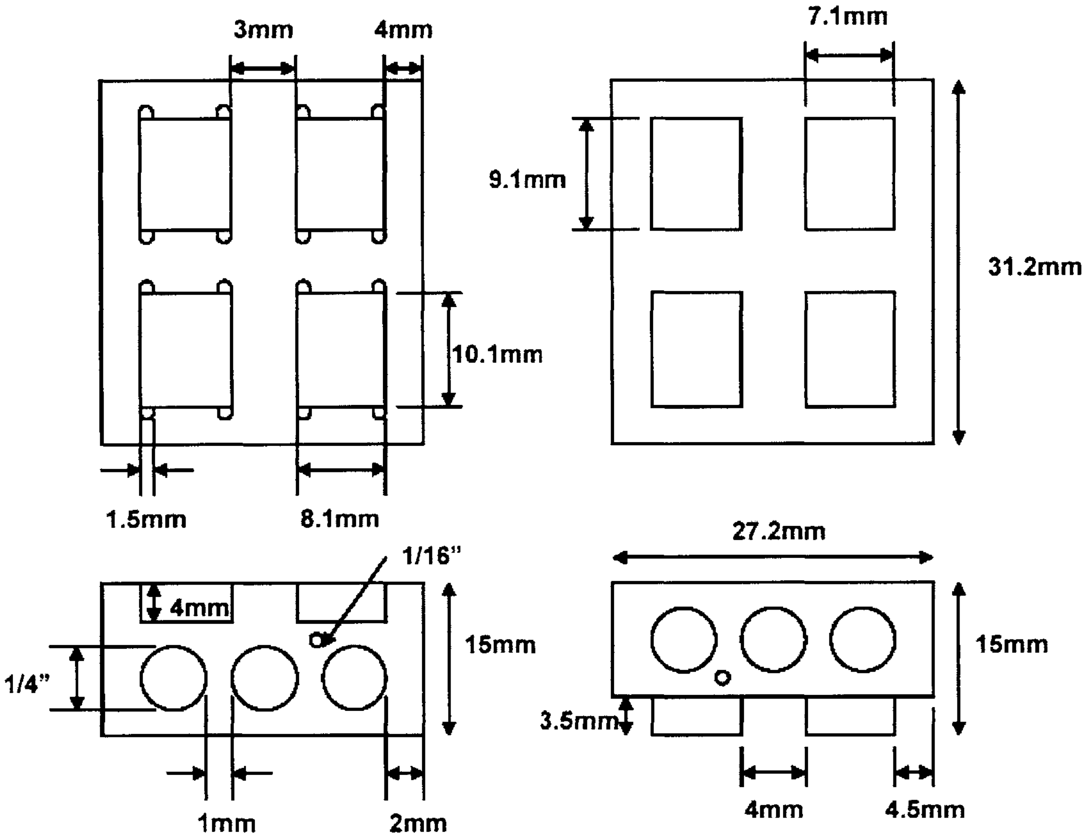

Figure E-1. Copper Vacuum Bonding Chuck

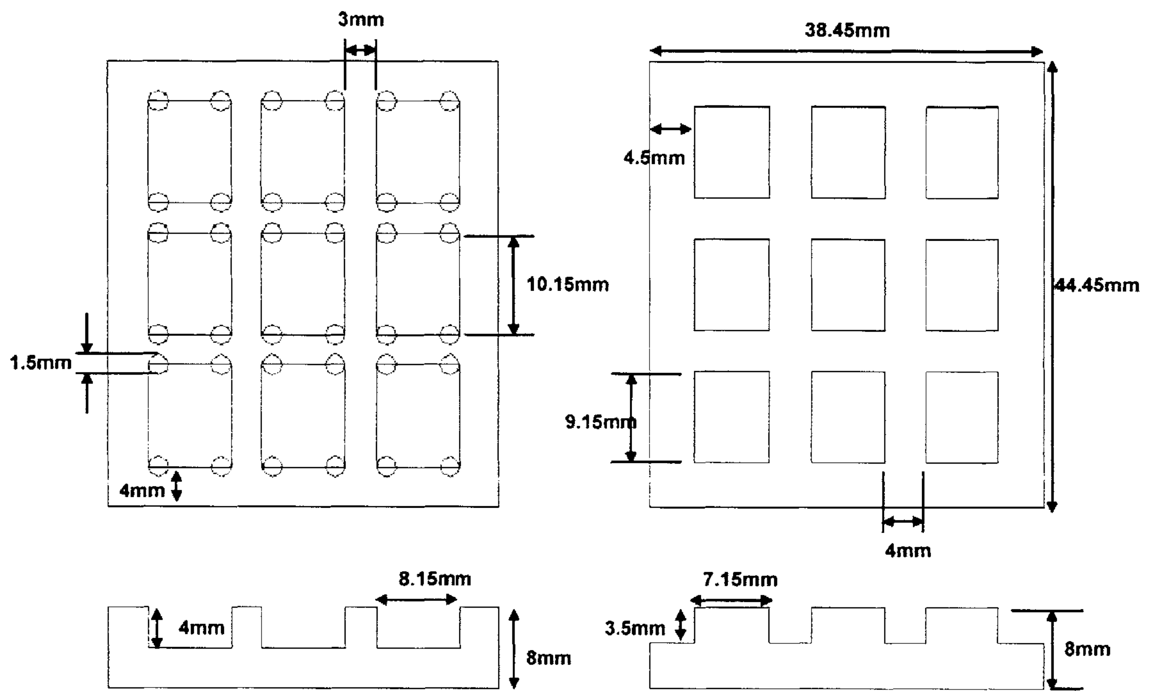

Figure E-2. Stainless Steel Bonding Chuck

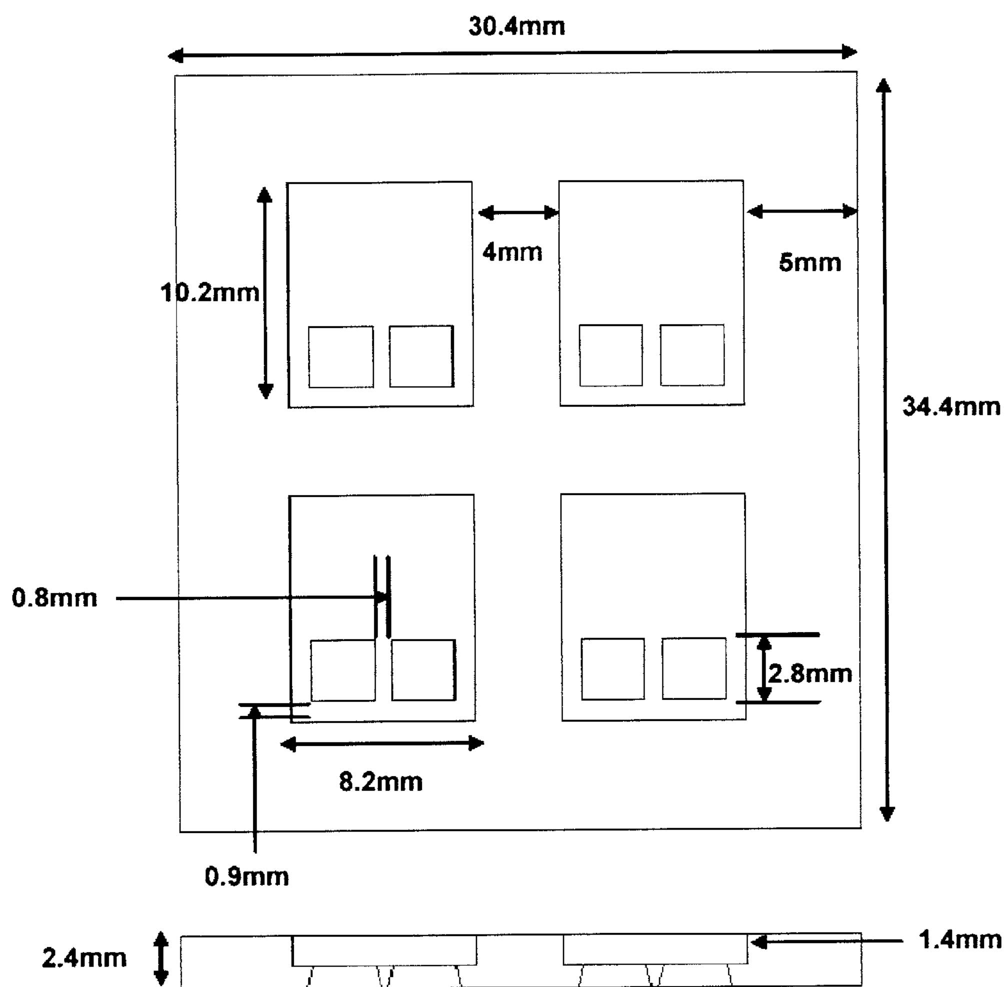

Figure E-3. Aluminum Shadow Mask

Appendix F
Optimization Images

The images utilized in the work for the vacuum bond optimization of Chapter 3, and the box bond optimization mention in Chapter 6 is compiled in this appendix. Tables F-1, F-2, and F-3 are included to summarize the pre-sintering and bonding conditions explored. The width of all the magnified images below spans a length of 2mm.

Vacuum Bonding Optimization

Table F-1. Presintering Conditions

Condition	Ramp Up	Peak Temp	Hold Time	Ramp Down	Ambient
PS01	90 min	520°C	30 min	120 min	Air
PS02	90 min	520°C	60 min	120 min	Air
PS03	90 min	520°C	120 min	120 min	Air
PS04	90 min	~500-540°C	30 min	~120 min	Vacuum
PS05	90 min	~500-540°C	60 min	~120 min	Vacuum
PS06	90 min	~500-540°C	120 min	~120 min	Vacuum
PS07	90 min	520°C	120 min	180 min	Inert (N_2)
PS08	90 min	300°C	30 min	180 min	Air
PS09	90 min	300°C	60 min	180 min	Air
PS10	30 min	450°C	60 min	180 min	Air
PS11	30 min	520°C	60 min	180 min	Air
PS12	30 min	500°C	60 min	180 min	Air
PS13	30 min	475°C	60 min	180 min	Air
PS14	30 min	490°C	60 min	180 min	Air
PS15	30 min	490°C	600 min	180 min	Air
PS16	30 min	450°C	600 min	180 min	Air
PS17	30 min	300°C	600 min	180 min	Air

PS01

PS01 - Magnified

PS02

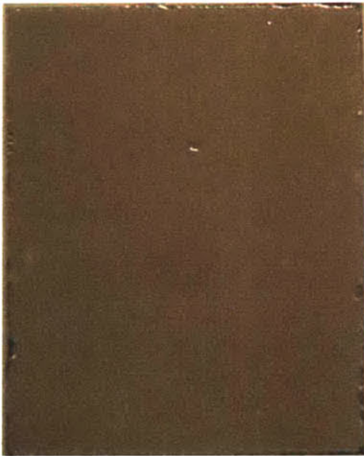

PS02 - Magnified

PS03

PS03 - Magnified

PS04

PS04 - Magnified

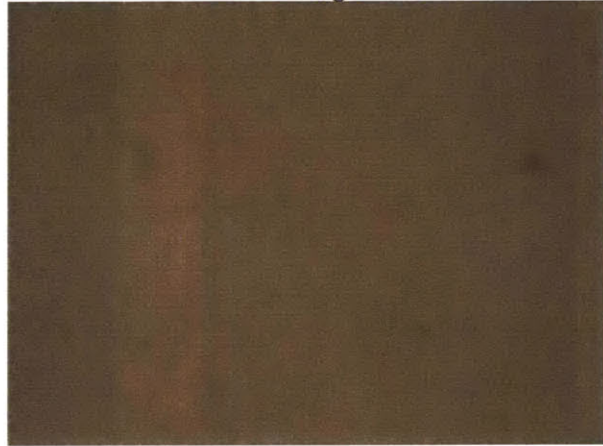

PS05

PS05 - Magnified

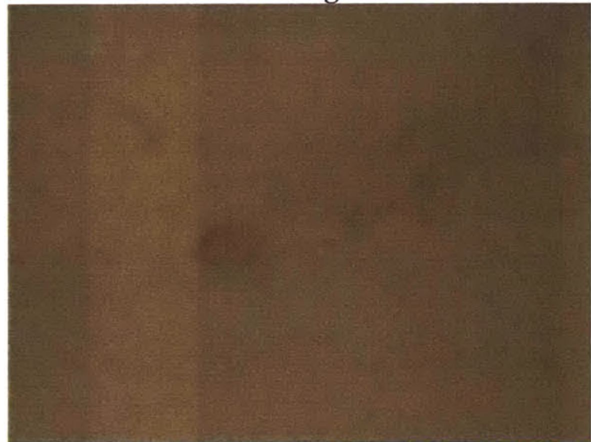

PS06

PS06 - Magnified

PS07

PS07 - Magnified

PS08

PS08 - Magnified

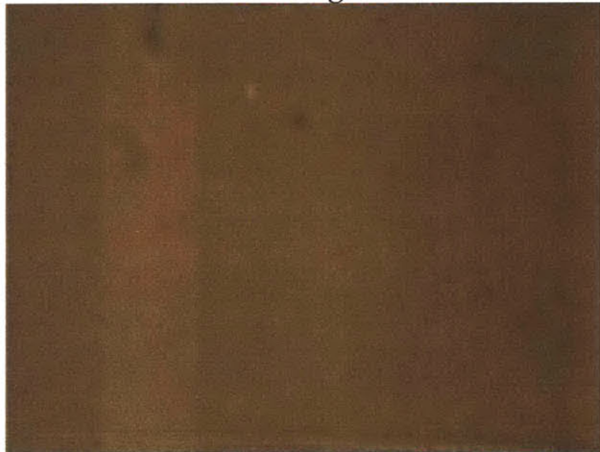

PS09

PS09 - Magnified

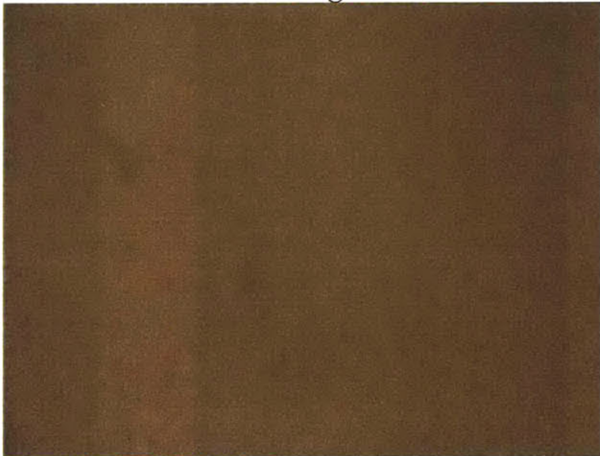

PS10

PS10 - Magnified

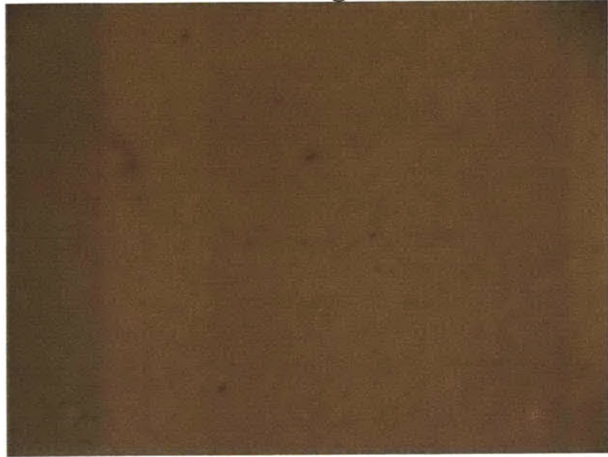

PS11

PS11 - Magnified

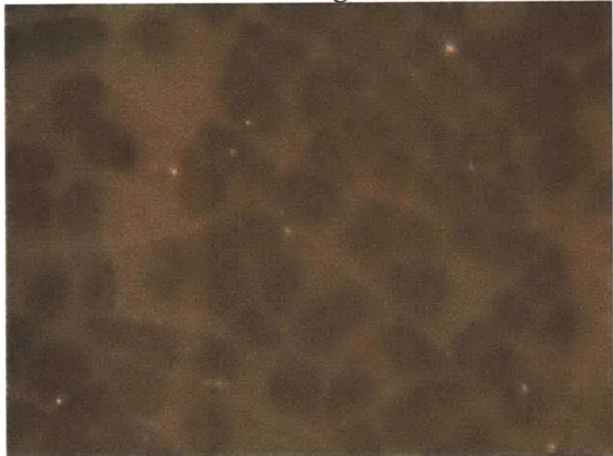

PS12

PS12 - Magnified

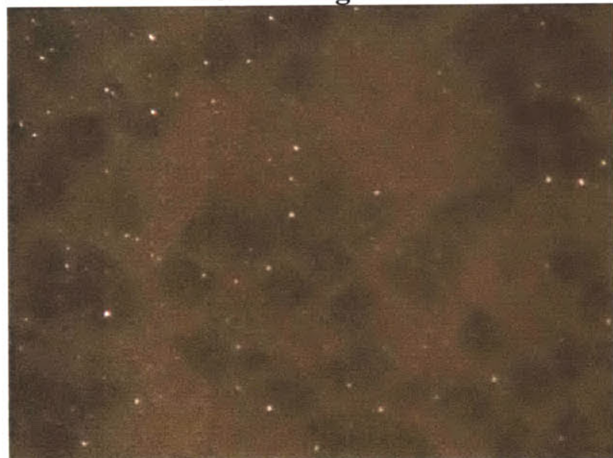

PS13

PS13 - Magnified

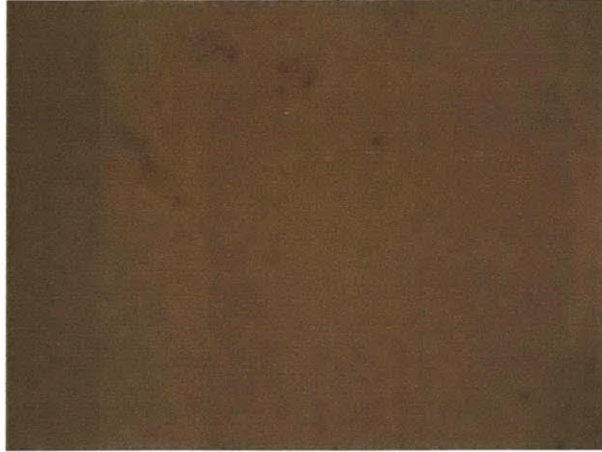

PS14

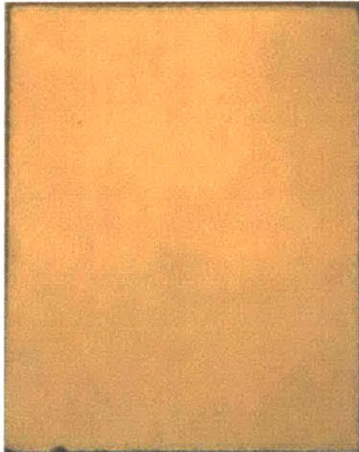

PS14 - Magnified

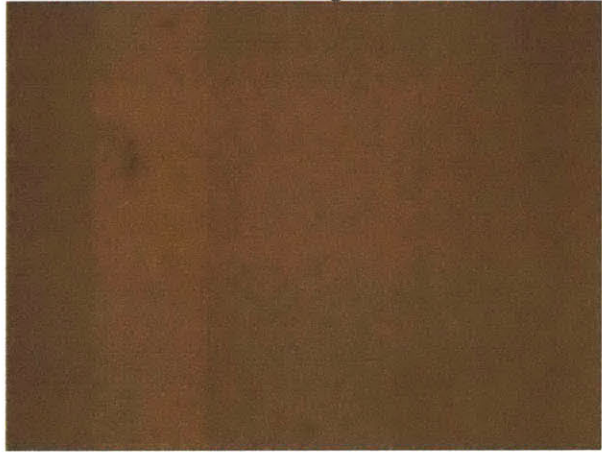

PS15

PS15 - Magnified

PS16

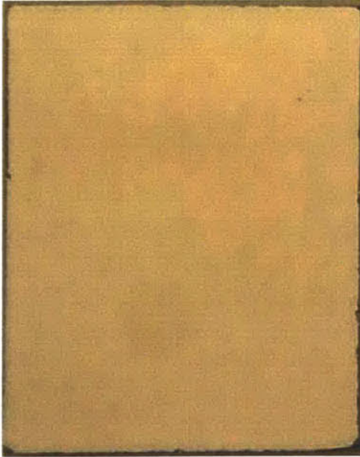

PS16 - Magnified

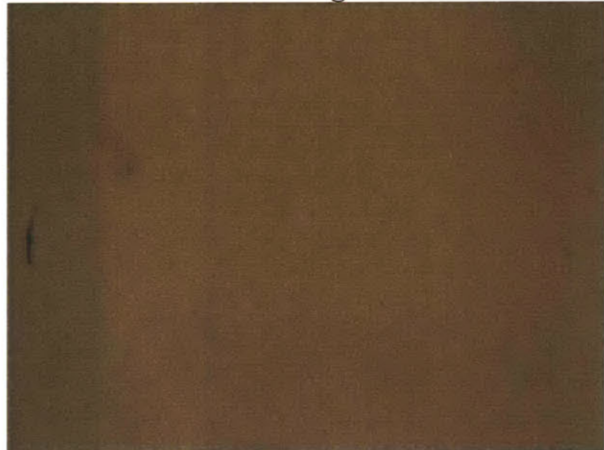

PS17

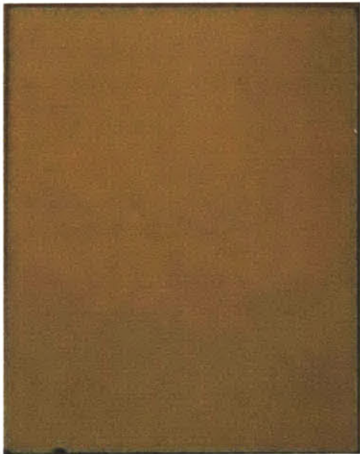

PS17 - Magnified

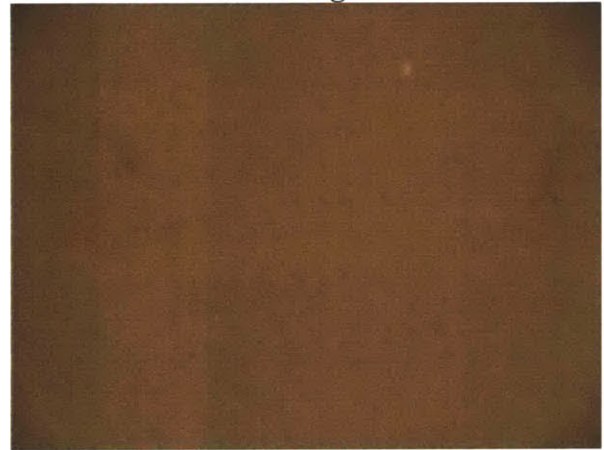

Un-sintered

Un-sintered - Magnified

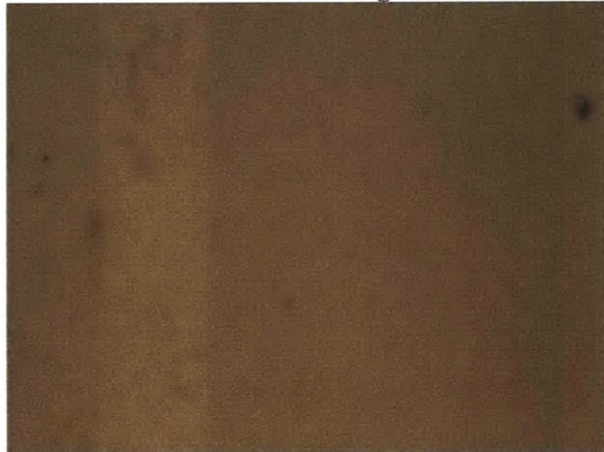

Table F-2. Vacuum Bonding Conditions							
Condition	**First Ramp**	**Outgas Temp**	**Outgas Time**	**Second Ramp**	**Bond Temp**	**Bond Time**	**Weights**
VB01	30 min	300°C	60 min	60 min	600°C	15 min	5kg
VB02	30 min	300°C	60 min	60 min	600°C	15 min	2kg
VB03	30 min	400°C	60 min	60 min	600°C	15 min	5kg
VB04	30 min	400°C	30 min	30 min	500°C	60 min	5kg
VB05	30 min	300°C	30 min	15 min	450°C	45 min	5kg
VB06	30 min	300°C	60 min	15 min	500°C	15 min	5kg
VB07	30 min	350°C	60 min	15 min	500°C	30 min	5kg

PS01+VB01

PS01+VB01 - Magnified

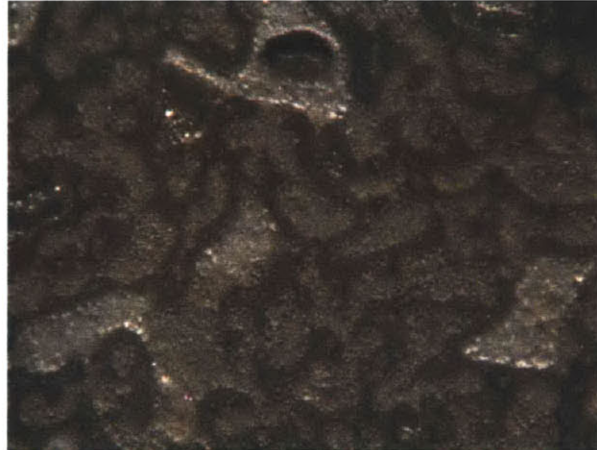

PS02+VB01

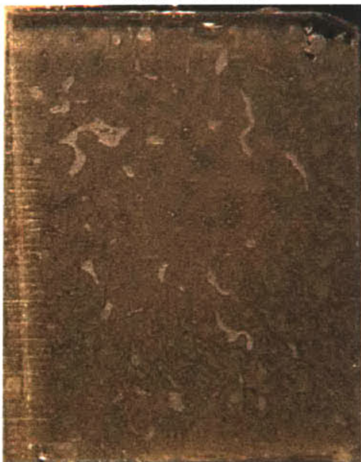

PS02+VB01 - Magnified

PS04+VB01

PS04+VB01 - Magnified

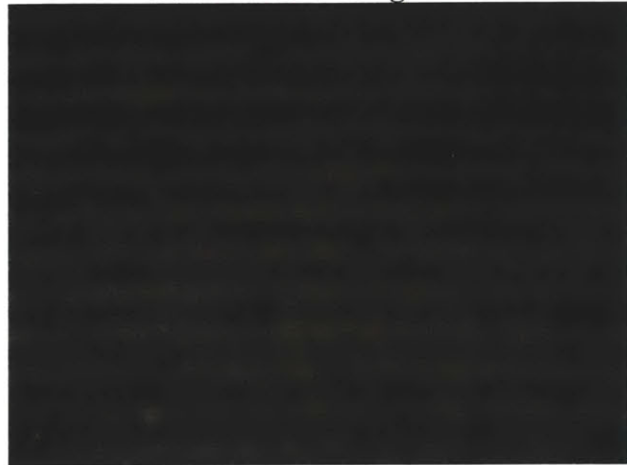

Un-sintered+VB01

Un-simtered+VB01 - Magnified

PS01+VB02

PS01+VB02 - Magnified

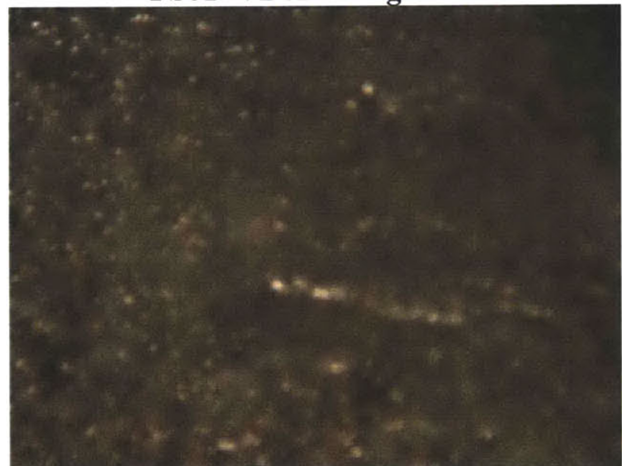

PS02+VB02

PS02+VB02 - Magnified

PS04+VB02

PS04+VB02 - Magnified

Un-sintered+VB02

Un-simtered+VB02 - Magnified

PS03+VB01

PS03+VB01 - Magnified

PS05+VB01

PS05+VB01 - Magnified

PS08+VB01

PS08+VB01 - Magnified

PS09+VB01

PS09+VB01 - Magnified

PS07+VB03

PS07+VB03 - Magnified

PS10+VB03

PS10+VB03 - Magnified

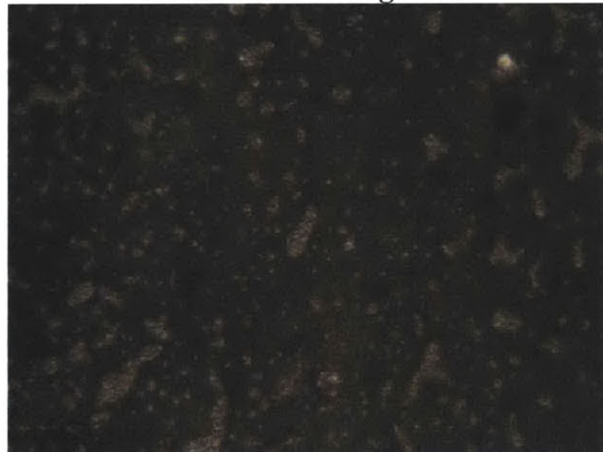

PS16+VB03

PS16+VB03 - Magnified

PS16+VB04

PS16+VB04 - Magnified

PS16+VB06

PS16+VB06 - Magnified

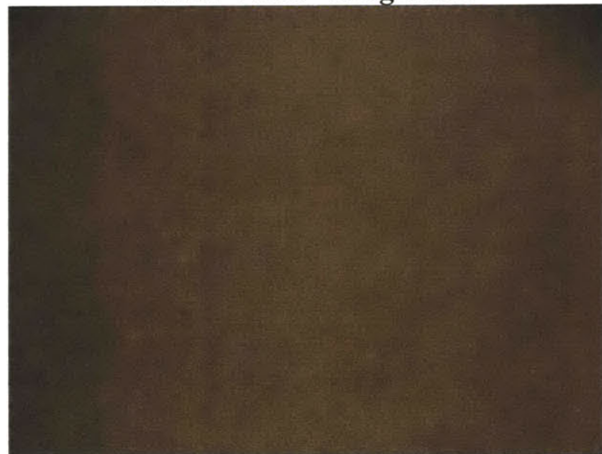

PS16+VB07

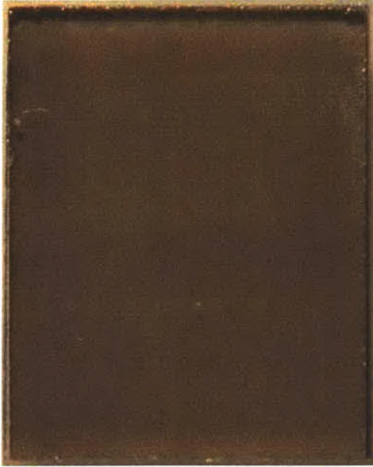

PS16+VB07 - Magnified

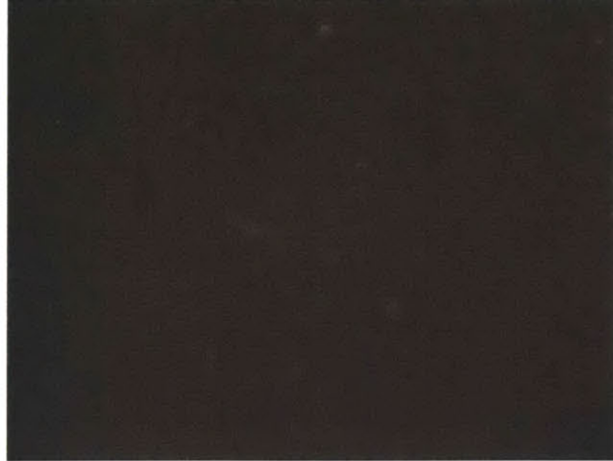

Box Furnace Bond Optimization

Table F-3. Box Bond Conditions					
Condition	**Ramp Up**	**Peak Temp**	**Hold Time**	**Ramp Down**	**Weights**
FB01	50 min	575°C	15 min	180 min	0.5kg
FB02	50 min	520°C	15 min	180 min	0.5kg
FB03	50 min	525°C	30 min	180 min	0.5kg
FB04	50 min	525°C	30 min	180 min	1.0kg
FB05	50 min	550°C	30 min	180 min	0.5kg
FB06	50 min	550°C	30 min	180 min	1.0kg
FB07	50 min	500°C	30 min	180 min	0.5kg
FB08	50 min	500°C	30 min	180 min	1.0kg
FB09	50 min	525°C	60 min	180 min	0.5kg
FB10	50 min	525°C	60 min	180 min	1.0kg
FB11	50 min	500°C	120 min	180 min	1.0kg

It may be noticed that the amount of weights used in this bond optimization work is significantly less than the amount used for the vacuum bond optimization. The reason for this difference is that the vacuum bonding chuck required the bonding of four samples simultaneously, reducing the effective applied pressure induced by the weights. For this work, each sample was bonded individually so a large amount of weights was not necessary. Upon careful observation, condition FB04 produces a bond that appears voidless, and is comparable in quality to the optimized vacuum bond.

FB01

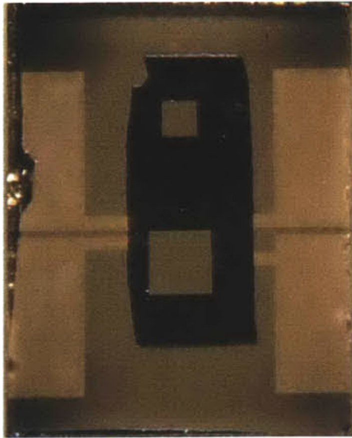

FB01 - Magnified

FB02

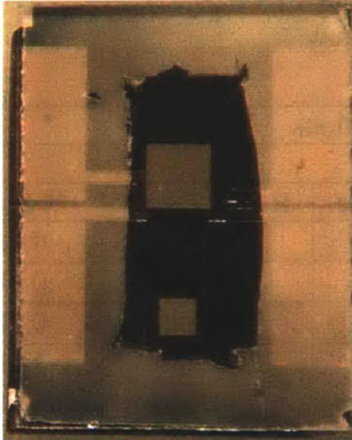

FB02 - Magnified

FB03

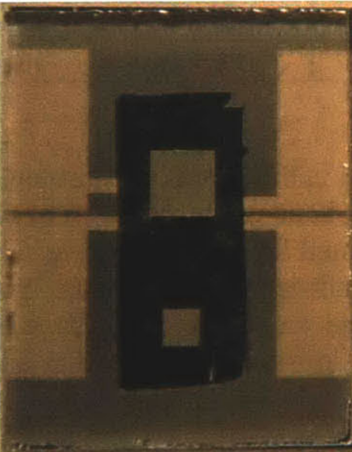

FB03 - Magnified

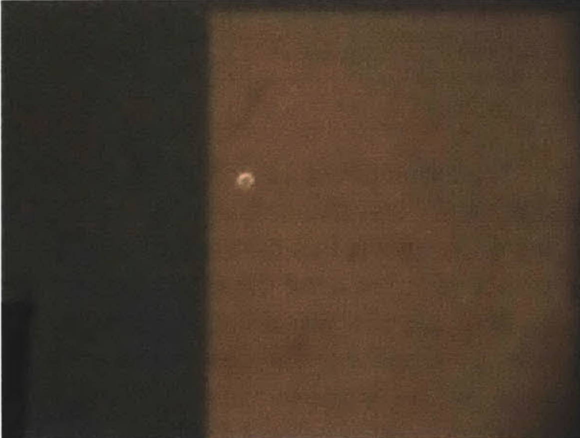

FB04

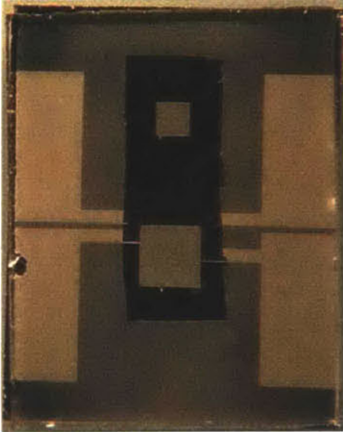

FB04 - Magnified

FB05

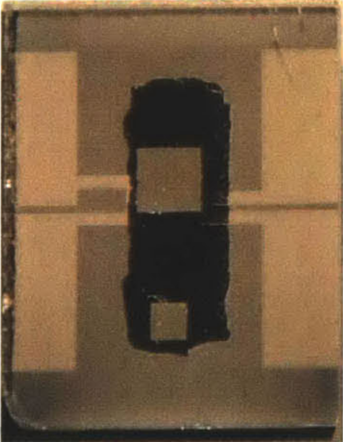

FB05 - Magnified

FB06

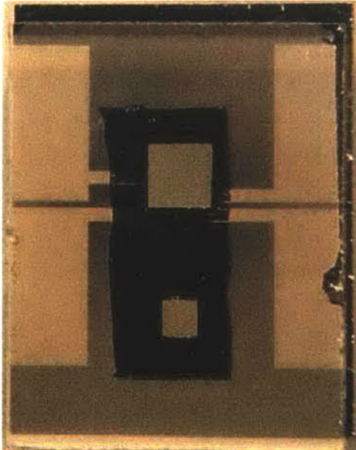

FB06 - Magnified

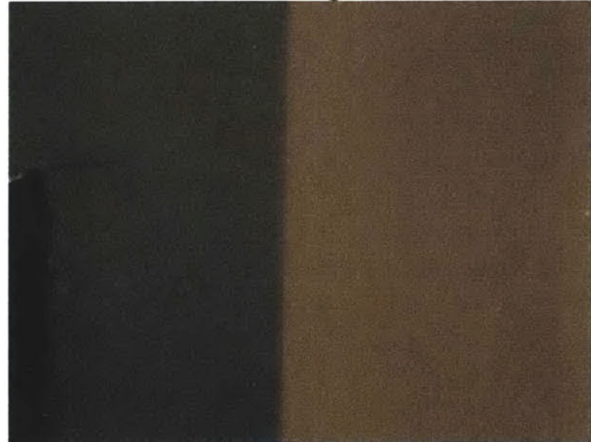

FB07

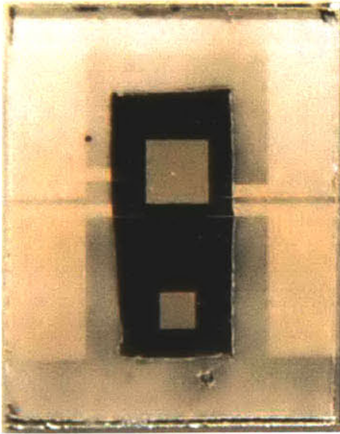

FB07 - Magnified

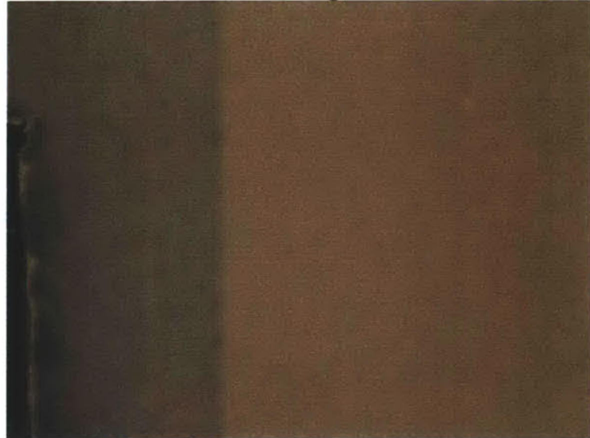

FB08

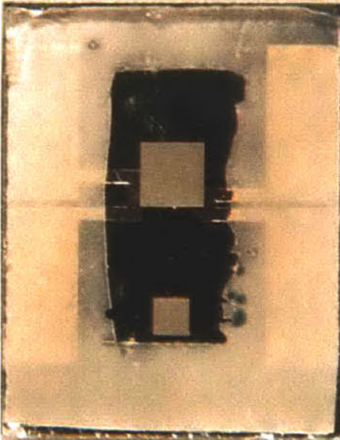

FB08 - Magnified

FB09

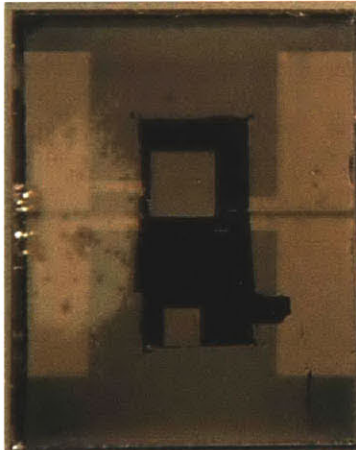

FB09 - Magnified

FB10

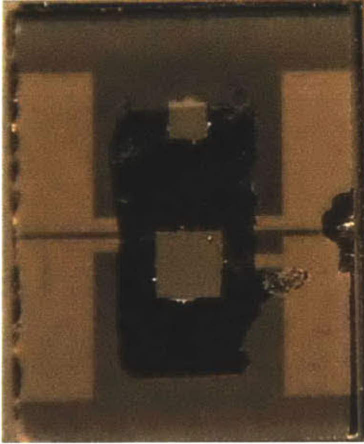

FB10 - Magnified

FB11

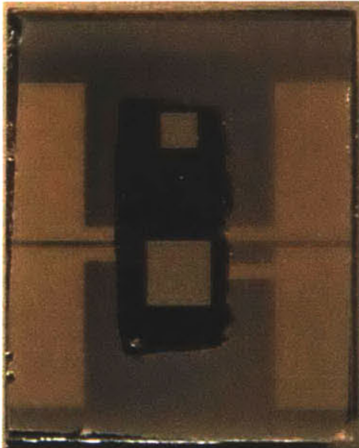

FB11 - Magnified

References

[1] L.R. Arana, "High-Temperature Microfluidic Systems for Thermally-Efficient Fuel Processing," PhD in ChemE Thesis, MIT, 2003.

[2] M.A. Schmidt, "Wafer-to-Wafer Bonding for Microstructure Formation," Proceedings of the IEEE, Volume 86, Number 8, August 1998.

[3] B. Lee, S. Seok, K. Chun, "A Study on Wafer Level Vacuum Packaging for MEMS Devices," Journal of Micromechanics and Microengineering, Volume 13, pp. 663-669, 2003.

[4] Y.T. Cheng, L. Lin, K. Najafi, "Localized Silicon Fusion and Eutectic Bonding for MEMS Fabrication and Packaging," Journal of Microelectromechanical Systems, Volume 9, Number 1, pp. 3-8, March 2000.

[5] D. Sparks, G. Queen, R. Weston, G. Woodward, M. Putty, L. Jordan, S. Zarabadi, K. Jayakar, "Wafer-to-Wafer Bonding of Nonplanarized MEMS Surfaces using Solder," Journal of Micromechanics and Microengineering, Volume 11, pp. 630-634, 2001.

[6] C.H. Tsau, M. Spearing, M.A. Schmidt, "Fabrication of Wafer-Level Thermocompression Bonds," Journal of Microelectromechanical Systems, Volume 11, Number 6, pp. 641-647, December 2002.

[7] S. Wilfert, C. Edelmann, "Miniaturized Vacuum Gauges," Journal of Vacuum Science Technology A, Volume 22, Number 2, Mar/Apr 2004.

[8] J. Chou, "A Study of Vacuum Packaging Methods for a Microfabricated Suspended Tube Reactor," MEng in EECS Thesis, MIT 2002.

[9] S.N. Cha, B.G. Song, N.S. Park, J.Y. Choung, J.E. Jung, N.S. Lee, J.M. Kim, J.H. You, L.H. Cho, J.H. Han, J.K. Chee, J.P. Hong, "Vacuum Packaging and Non-evaporable Getter Activation for Field Emission Display by a Continuous Wave Infrared Laser."

[10] D.J Lee, Y.H. Lee, G.J. Moon, J.D. Kim, W.D. Choi, S.G. Lee, J. Jang, B.K. Ju, "Vacuum Packaging Technology of AC-PDP using Direct-Joint Method," Journal of Information Display, Volume 2, Number 4, 2001.

[11] D.J. Lee, Y.H. Lee, B.K. Ju, G.J. Moon, J.D. Kim, M.H. Oh, J. Jang, "Development of In-line Sealing Method for Plasma Display Panel," Society of Information Displays Digest, 2002.

[12] S.J. Kwon, H.C. Yang, K.W. Whang, "Plasma Display Panel Vacuum In-line Sealing Technology Using a Bubble-Reduced Frit," Journal of Vacuum Science Technology A, Volume 21, Number 1, Jan/Feb 2003.

[13] K.S.Ryu, S.J. Kwon, "Glass Packaging of the 0.7 Inch Diagonal FED Panel," SMDL Annual Report, 1998.

[14] S.J. Kwon, K.J. Hung, J.D. Lee, C.W. Oh, J.S. Yoo, Y.B. Kwon, "Influence of Getter Activation and Aging in a Frit-Sealed Field Emission Display Panel," Journal of Vacuum Science Technology B, Volume 18, Number 3, May/Jun 2000.

[15] G. Chen, "Nanoscale Energy Transport and Conversion," pp. 282-323, 2004.

[16] G. Chen., D. Borca-Tasciuc, R.G. Yang, "Nano Heat Transfer," Encyclopedia of Nanoscience and Nanotechnology, Cambridge, USA, American Scientific Publishers, Volume 10, pp. 1-30, 2004.

[17] W. Holmes, J.M. Gildemeister, P.L Richards, "Measurement of Thermal Transport in Low Stress Nitride Films," Applied Physics Letters, Volume 72, Number 18, pp. 2250-2252, 1998.

[18] B.L. Zink, F. Hellman, "Specific Heat and Thermal Conductivity of Low-Stress Amorphous Si-N Membranes," Solid State Communications, Volume 129, pp. 199-204, 2004.

3506-53